integration of HPV genome into the host DNA causes malignant transformation through the integration of viral E6 and E7 oncogenes into the host genome; these oncogenes deregulate the cell cycle regulators p53 and retinoblastoma proteins [2, 3]. However, most infections resolve spontaneously and pass uneventfully. Progression of low-grade squamous intraepithelial lesions (LSILs) to high-grade squamous intraepithelial lesions (HSILs) and subsequent invasion is linked to the persistence of HPV infection and to genetic and/or epigenetic alteration(s), which may act synergistically or independently [4].

A disintegrin and metalloproteases (ADAMs) are transmembrane proteins with broad tissue distribution. The structure of ADAMs is closely related to that of snake venom proteins [5]. ADAMs are multidomain proteins that comprise a prodomain, a zinc metalloprotease domain, a disintegrin domain, a cysteine-rich region, an epidermal growth factor-like region, a transmembrane domain and a cytoplasmic domain.

The ADAM with thrombospondin motif (ADAMTS) family of proteins is structurally related to ADAMs; however, they lack epidermal growth factor-like sequences and the transmembrane domains and are characterized by the presence of a variable number of thrombospondin-like motifs. Hence, they are soluble secreted proteins [6]. ADAMs play critical roles in physiological, inflammatory and pathological conditions through ectodomain shedding of cell ligands and the modulation of cell-cell and cell-matrix interactions [7–9]. ADAMs are involved in specific cellular processes including fertilization, neurogenesis and adipogenesis [10–13].

An increasing body of evidence indicates that disintegrin-metalloprotease proteins are involved in the formation and progression of a variety of cancers [14, 15] through regulation of cell adhesion, migration and invasion. ADAMTS-1 was found to be a regulator of metastasis depending on its catalytic domain and protein status [16, 17]. Taken together, these findings may suggest a pivotal role of ADAMs and ADAMTSs as a distinct group of oncogenes or tumor suppressor proteins [18]. Disintegrin-metalloprotease molecules share structural homology with the matrix metalloproteases (MMPs), a family of zinc-dependent proteases, in that they share a metalloprotease domain. However, half of ADAMs exert catalytic activities [19, 20]. Tissue inhibitors of metalloproteases (TIMPs), known to be potent physiological inhibitors of MMPs, can also selectively regulate the activities of specific ADAMs and ADAMTSs [21–23].

The molecular mechanisms underlying progression from normal epithelium through preinvasive cervical lesions to invasion are complex and poorly understood. Proteolysis, due to upregulation of proteases, is one of the hallmarks of cancer progression [24]. Members of the MMP family are implicated in the pathogenesis and progression of cervical carcinoma [25, 26]. Because of the close similarity between MMPs and the disintegrin-metalloprotease family, we speculated that ADAMs and ADAMTSs might play a role in cervical tumorigenesis.

Materials and Methods

Cell Lines

The cervical cancer cell lines of the squamous type (QG-U, SKG-IIIb and Yumoto) were kindly provided by Dr. Minoru Ueki (Osaka Medical College, Osaka, Japan) [27]. QG-U and SKG-IIIb cell lines are HPV positive, while the Yumoto cell line is HPV negative [28]. Cells were cultured in RPMI-1640 (Nissui, Tokyo, Japan) supplemented with 10% heat-inactivated fetal bovine serum (Biowest, Tokyo, Japan) and cultured at 37°C with 5% CO_2. The in vitro multistep cervical carcinogenesis model was chosen to assess the expression profile of proteases at the mRNA and protein levels during the course of cervical carcinogenesis. The model of oncogenically modified human cervical keratinocytes has been thoroughly described in previous literature [29]. Briefly, human cervical keratinocytes (HCK) were obtained from donors with informed consent. Keratinocytes were sequentially transduced with hTERT, HPV-16 E6E7 (viral oncoproteins) and/or oncogene(s) of interest such as Hras and c-Myc. Immortalized HCK transduced with HPV-16 E6E7 have similar characteristics to LSILs. HCK transduced with E6E7 and Hras oncogenes are similar to HSILs. Immortalized HCK with E6E7/Hras/c-Myc oncogenes had features of invasive cervical cancer. The latter 2 types of oncogenically modified cells were confirmed to be resistant to contact inhibition and differentiation. Cells were grown in defined keratinocyte serum-free medium (Gibco, New York, N.Y., USA) supplemented with growth supplement (Gibco) and cultured at 37°C with 5% CO_2.

RNA Extraction and Reverse Transcription Polymerase Chain Reaction

Total RNA was extracted using sepasol-RNA I (Nacalai Tesque, Kyoto, Japan). Genomic DNA contamination was eliminated by use of DNase (Promega, Madison, Wisc., USA). A volume of 5 μg of total RNA measured with a U-1800 spectrophotometer (Epson, Japan) was reverse transcribed with 5 units of reverse transcriptase (RT; Promega) and mixed with 0.5 μg of oligo (dT), 5 μl of 5× buffer, 2 μl of 2 mM deoxynucleotide triphosphate mixture and 40 units of RNasin. The resulting mixture (25 μl) was incubated at 42°C for 60 min and then at 65°C for 15 min. A thermal cycler (GeneAmp® PCR System 9700, PE Applied Biosystems) was used for the PCR reaction. In a PCR tube, 12.5 μl of Amplitaq Gold® PCR master Mix (Roche, N.J., USA), 9.5 μl of distilled water, 1 μl of each specific paired primer (Operon, Japan) and 1 μl of cDNA were mixed together. The primer sequences are given in table 1. The resultant mixture was denatured at 95°C for 5 min, followed by cycles of 30 s at 95°C, 45 s at the respective annealing temperature (table 1) and 1 min at 72°C as an extension

Table 1. The primer sequences designed for the RT-PCR analysis

Target gene		Primer sequence	Cycles n	Tm °C	Product size, bp
ADAM-9	forward	5′-GCTAGTTGGACTGGAGATTTGG-3′	30	57.7	486
	reverse	5′-TTATTACCACAGGAGGGAGCAC-3′		57.7	
ADAM-10	forward	5′-AATTCTGCTCCTCTCCTGGGC-3′	30	59.5	299
	reverse	5′-TATGTCCAGTGTAAATATGAGAGG-3′		54.4	
ADAM-12 L	forward	5′-CCAGAACAACTCGGCTCACT-3′	28	57.5	481
	reverse	5′-AGGCCTTGATCAGAAAGCAA-3′		53.4	
ADAM-12 S	forward	5′-TCAGTGCTGCTCCTGAGAGA-3′	28	57.5	449
	reverse	5′-AAGGGTTGGTGACTCTGTGG-3′		57.5	
ADAM-15	forward	5′-CAAATATAGGTGGCACTGAGGAG-3′	30	57.8	286
	reverse	5′-TAGCAGCAGTTCTCCAAAGTGTG-3′		57.8	
ADAM-17	forward	5′-ATGAGGCAGTCTCTCCTATTCCTGAC-3′	28	61.2	456
	reverse	5′-AAGTGGCTCTATGTTATATTCGGCCC-3′		59.6	
ADAMTS-1	forward	5′-ACGGCAGTGGTCTAAAGCAT-3′	30	55.4	312
	reverse	5′-AGTTCCAACATCAGCCATCC-3′		55.4	
ADAMTS-2	forward	5′-CTACGTCCAGAGCAGGGGTA-3′	30	59.5	336
	reverse	5′-GAACTCCTCCTCCTCCATCC-3′		59.5	
ADAMTS-3	forward	5′-TAGAAAGGGGAAACCCATCC-3′	30	55.4	243
	reverse	5′-CCCGTTTCATGGGCTACTAC-3′		57.5	
ADAMTS-4	forward	5′-TGCATCTGCCTGTGACTTTC-3′	30	55.4	433
	reverse	5′-GTTGGGCAGTCCTCAGTGTT-3′		57.5	
ADAMTS-5	forward	5′-GGACCTACCACGAAAGCAGA-3′	30	57.5	411
	reverse	5′-CCTCTTCCCTGTGCAGTAGC-3′		59.5	
ADAMTS-8	forward	5′-ACTGACATGGACGGGAATCT-3′	30	55.4	216
	reverse	5′-GAGTCCACCACATGGTCACA-3′		57.5	
ADAMTS-9	forward	5′-TCGCTCCACTGTTCACTGTC-3′	28	57.5	297
	reverse	5′-CCTGTTGAGGGCTCTCTCTG-3′		59.5	
ADAMTS-15	forward	5′-CTCCAAGCCCTGTCCTTACA-3′	30	57.5	337
	reverse	5′-CCAGATTGCAGGATCGGTAT-3′		55.4	
TIMP-1	forward	5′-TGGCACTCATTGCTTGTGGACG-3′	28	58	203
	reverse	5′-TCCGGAAGAAAGATGGGAGTGGGA-3′		58.8	
TIMP-2	forward	5′-TTCTGCACGGGGCTTTCTGCAT-3′	28	57	528
	reverse	5′-TGCTTTGGGGTTGCCGCTGAAT-3′		57	
TIMP-3	forward	5′-TCCTGAACCGTGTTTGTTGA-3′	28	59.5	249
	reverse	5′-CTTGACTGTGCTTGGTGGAA-3′		58.9	
β-Actin	forward	5′-CGCCGCCAGCTCACCATGGA-3′	30	59	611
	reverse	5′-CTGTAGCCGCGCTCGGTGAG-3′		59	

Tm = Melting temperature; ADAM-12 L = long isoform of ADAM-12; ADAM-12 S = short isoform of ADAM-12.

step. Using electrophoresis, the PCR products were run on 1.2% agarose gel and visualized with ethidium bromide stain.

Real-Time PCR

The mRNA expression levels of selected ADAMs, ADAMTSs and TIMPs were quantified by real-time PCR and normalized to the mRNA expression level of glyceraldehyde-3-phosphate dehydrogenase (GAPDH). Sequences of the primers used are shown in table 2. PCR reactions were run in a LightCycler 480 System (Roche) and carried out in a 96-well PCR plate format. Volumes of 17 μl of LightCycler SYBR Green I Master mix (Roche), 0.5 μM forward and reverse primer and 1 μl of cDNA template (20 μl in total) were made and mixed well. The thermal profile of real-time PCR reactions was as follows: heating at 95°C for 10 min followed by 50 cycles of 10 s of denaturation at 95°C, 20 s at the respective annealing temperature (table 2) and 10 s of amplification at 72°C. Experiments were performed in triplicate, and samples were subjected to agarose gel electrophoresis and ethidium bromide visualization to exclude nonspecific PCR. The fluorescence emitted from the SYBR green dye was read by the instrument after completion of each cycle, and the results were normalized to the mRNA expression of GAPDH.

Table 2. The primer sequences designed for the real-time RT-PCR analysis

Target gene		Primer sequence	Cycles, n	Tm, °C	Product size, bp
ADAM-9	forward	5′-TGGAACTGCAGGAATGGCA-3′	50	58	72
	reverse	5′-CCAAACACATTAATCCCGCC-3′		58	
ADAM-10	forward	5′-ACAGCCCATTCAGCAACCC-3′	50	57	67
	reverse	5′-GCGTCTCATGTGTCCCATTTG-3′		57	
ADAM-12 L	forward	5′-AGGCCAGAGCCAAGGGGCTT-3′	50	60	88
	reverse	5′-TGGGAGCCTGCCTGCCAGTT-3′		60	
ADAM-12 S	forward	5′-TACCACTCTGGCAGGCCCCA-3′	50	59	111
	reverse	5′-ACACTGGGCCCAACCCTTGC-3′		59	
ADAMTS-1	forward	5′-CGTCTCACCAAAGGACAGGT-3′	50	58	114
	reverse	5′-GAGGTGGAATCTGGGCTACA-3′		58	
TIMP-1	forward	5′-TCTGAAAAGGGCTTCCAGTCCCGT-3′	50	59	95
	reverse	5′-ATTCAGGCTATCTGGGACCGCA-3′		58	
TIMP-2	forward	5′-AATGAAACCGAAGCTTGGCGGC-3′	50	59	92
	reverse	5′-TGCTTTGGGGTTGCCGCTGAAT-3′		59	
TIMP-3	forward	5′-CTTTCTCCTCTGTGCCTGCT-3′	50	59	86
	reverse	5′-CTTGACTGTGCTTGGTGGAA-3′		59	
GAPDH	forward	5′-CAATGACCCCTTCATTGACC-3′	50	59	159
	reverse	5′-TTGATTTTGGAGGGATCTCG-3′		59	

Tm = Melting temperature; ADAM-12 L = long isoform of ADAM-12; ADAM-12 S = short isoform of ADAM-12.

Antibodies

Commercially available antibodies used were as follows: mouse antihuman ADAM-9 directed against the ectodomain (R&D), goat anti-ADAM-9 polyclonal antibody directed against the C terminus (Santa Cruz, USA), rabbit antihuman ADAM-10 polyclonal antibody directed against the C terminus (Millipore, USA), rabbit antihuman ADAM-12 directed against the cytoplasmic domain (Triple Point Biologics, Forest Grove, Oreg., USA), rabbit antihuman TIMP-2 polyclonal antibody (Chemicon, Temecula, Calif., USA), mouse antihuman TIMP-3 monoclonal antibody (Abcam, Tokyo, Japan) and mouse antihuman β-actin (Abcam).

Immunoblotting

Cell cultures were washed 3 times with phosphate-buffered saline and resuspended in lysis buffer containing 50 mM Tris-HCl (pH 8), 120 mM NaCl, 1 mM EDTA and 1% protease inhibitors (Calbiochem, USA). The cell lysates were centrifuged at 15,000 rpm for 10 min at 4°C, and the resultant supernatants were collected. Protein concentration was measured using the Bio-Rad protein assay (Hercules, Calif., USA). A total of 20 μg of protein sample was resolved using 10% SDS polyacrylamide gel electrophoresis and transferred onto methanol-pretreated polyvinylidene difluoride membranes (Millipore). Membranes were blocked with 5% nonfat milk and incubated with primary antibodies overnight at 4°C. The primary antibodies were used at the following dilutions: anti-ADAM-9, 1:500; anti-ADAM-10, 1:500; anti-ADAM-12, 1:1,000; anti-TIMP-2, 1:1,000; anti-TIMP-3, 1:1,000, and anti-β-actin, 1:3,000. The membranes were then washed 3 times in Tris-buffered saline containing 0.05% Tween and incubated for 1 h at room temperature in horseradish peroxidase-conjugated antirabbit or antimouse IgG at a dilution of 1:2,500. Chemiluminescent detection of horseradish peroxidase was achieved with Pierce Western blotting substrate (Thermo Scientific, USA) according to the manufacturer's instructions. The membranes were exposed to X-ray film, and the band densities were analyzed using NIH ImageJ software. Each value was normalized to the band density of the respective β-actin band.

Tissue Samples and Immunohistochemistry

Thirty-one formalin-fixed, paraffin-embedded cervical tissue blocks were obtained from the Department of Obstetrics and Gynecology of the Osaka Police Hospital. Histopathological diagnosis of each specimen was made independently by two pathologists. Tissue blocks were LSILs (n = 12), HSILs (n = 11) or invasive squamous cell carcinoma (n = 8). Informed consent was obtained from patients before the procedures, and the study was approved by the Osaka University review board. Tissue sections (4–5 μm) from representative paraffin blocks were deparaffinized in xylene and rehydrated in graded ethanol. The sections were subjected to heating in target retrieval buffer for 20 min. Endogenous peroxidases were blocked using 10% hydrogen peroxide for 15 min. Further blocking was carried out by incubating the sections with 5% bovine serum albumin for 30 min. The slides were then incubated with the primary antibody at 4°C in a moist chamber overnight. The primary antibodies were anti-ADAM-9 (1:50; R&D), anti-ADAM-10 (1:100; Millipore) and anti-TIMP-3 (1:100; Abcam). The slides were then incubated with specific secondary antibody at a dilution of 1:100 for 30 min at room temperature. The sections were incubated with streptavidin (Chemicon) at a dilution of 1:100 for 30 min. The sections were treated with 3,3′-diamino-

benzidine as a chromogen, and finally slides were counterstained with hematoxylin. Negative controls were included, with the omission of primary antibodies.

Evaluation of Immunoreactivity

The immunoreactivity was judged according to the distribution of staining (membranous, cytoplasmic and nuclear) and semiquantitative assessment of immunoreactivity, i.e. brown nuclear and cytoplasmic reactivity. A simplified scoring system was developed by calculating the percentage of immunoreactive cells. For each slide, nearly 3,000 cells were assessed for expression of a given antigen. The immunoreactivity was scored as negative (no reactive cells), weak (<10% reactive cells), moderate (11–50%) or strong (50–100%).

Statistical Analysis

Data from densimetric studies of multiple experiments were calculated for graphical depiction and statistical analysis. Student's t test was used to construct 95% confidence intervals for the differences in the various cell lines. ADAM expression in normal cervical tissue, LSILs, HSILs and cervical cancer was compared using analysis of variance. Statistical significance was defined by a p value of <0.05.

Results

Differential Expression of ADAM and ADAMTS mRNAs

To determine the expression of ADAMs and ADAMTSs in cervical cells, and to investigate their aberrant expression (if any) during cervical carcinogenesis, we performed conventional PCR analysis using an in vitro multistep carcinogenesis model of cervical cancer and human squamous cervical cancer cell lines.

ADAMs with an active catalytic domain, such as ADAM-9, -10, -12, -15 and -17, together with ADAMTS-1, -2, -3, -4, -5, -8, -9 and -15, were evaluated in our study. Levels of ADAM-9, -10 and -12 mRNAs were gradually upregulated in the oncogenically modified keratinocytes and in the cancer cell lines compared to the normal keratinocytes. ADAM-15 mRNA was detected only in normal keratinocytes and in the cancer cell lines (fig. 1).

Among the ADAMTSs tested, only ADAMTS-1 showed expression in carcinogenesis steps and in cancer cell lines (fig. 1). ADAMTS-3 mRNA was expressed in all the cancer cell lines, with no expression in the oncogenically modified cells. ADAMTS-2 mRNA was not detected in either of the groups. Some ADAMTSs were expressed sporadically in some cervical cancer cell lines (fig. 1).

To obtain more sensitive measurement, we performed real-time quantitative RT-PCR analysis using mRNAs from oncogenically modified cells and cervical cancer cell lines.

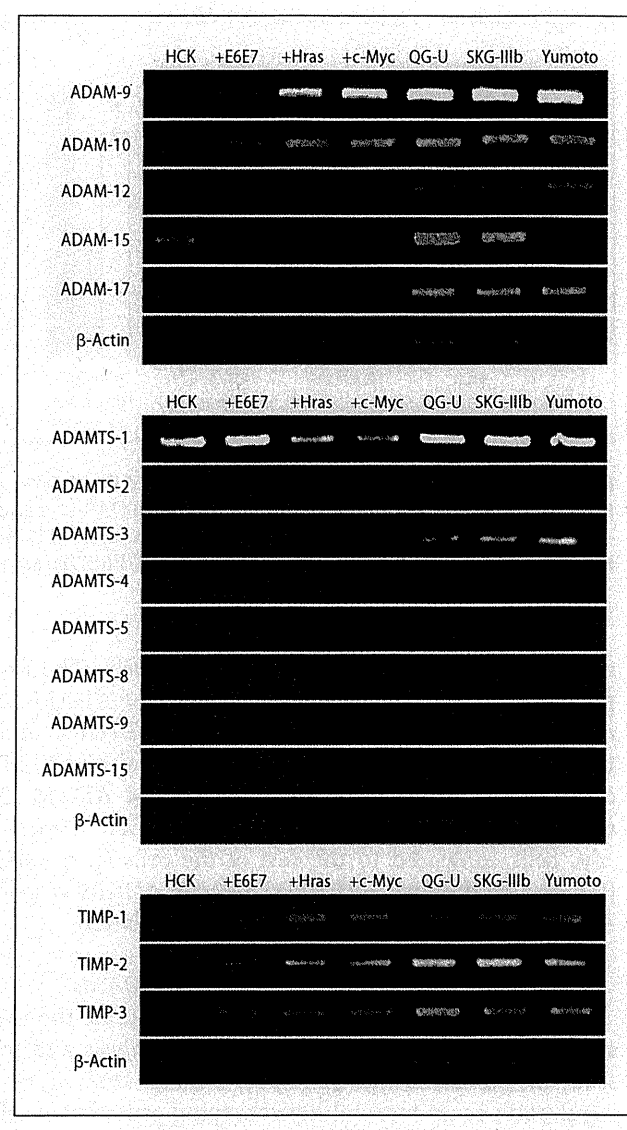

Fig. 1. RT-PCR analysis of ADAMs, ADAMTSs and TIMPs mRNA expression in normal keratinocytes (HCK = control cells), oncogenically modified keratinocytes (+E6E7 = LSILs; +Hras = HSILs; +c-Myc = invasive lesions) and squamous-type cervical cancer cell lines (QG-U, SKG-IIIb and Yumoto). The products were separated by agarose gel electrophoresis and stained with ethidium bromide.

The changes in ADAMs mRNA levels were normalized for levels of GAPDH mRNA in the same PCR. Alternative splicing of the ADAM-12 gene produces 2 isoforms, 1 long and 1 short; therefore, 2 pairs of primers were designed. A two-fold increase (a value of 2) or decrease (a value of 1) was considered target gene mRNA

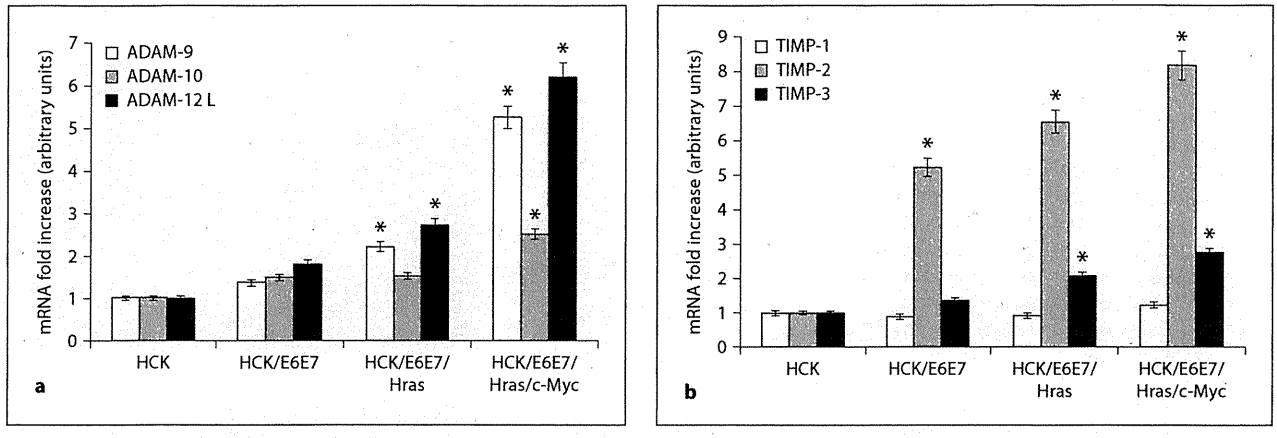

Fig. 2. Quantitative RT-PCR analysis of ADAM-9, ADAM-10 and the long form of ADAM-12 (ADAM-12 L) (**a**) and TIMP-1, -2 and -3 mRNAs (**b**) in oncogenically modified keratinocytes (HCK/E6E7 = LSILs; HCK/E6E7/Hras = HSILs; HCK/E6E7/Hras/c-Myc = invasive lesions) compared to control cells (HCK). Values for ADAMs and TIMPs in the different oncogenic stages were normalized relative to the expression levels of normal keratinocytes and normalized to the housekeeping gene (GAPDH). * $p < 0.05$.

upregulation or downregulation, respectively. The expression of ADAM-9 and the long form of ADAM-12 mRNA was significantly elevated in E6E7/Hras and E6E7/Hras/c-Myc cells compared to normal and E6E7 cells ($p < 0.05$; fig. 2a). The expression of ADAM-10 mRNA was significantly upregulated in E6E7/Hras/c-Myc cells compared to the rest of the cells ($p < 0.05$; fig. 2a). Quantitative PCR of ADAM-15, ADAM-17 and ADAMTS-1 did not show significant modulation.

Immunoblotting and Quantification of ADAMs

Immunoblotting was essential to corroborate the results obtained by quantitative RT-PCR analysis and to study the protein status. Quantitative image analysis, using β-actin as an internal housekeeping gene, was used to correct for protein loading between the control and test lanes in each experiment.

Immunoblotting of ADAM-9 protein showed 3 different bands, migrating with molecular masses of 114, 85 and 50 kDa, which represent the precursor, mature and processed forms of ADAM-9, respectively (fig. 3a, b). The ADAM-9 precursor form (114 kDa) was expressed in E6E7/Hras ± c-Myc-transduced keratinocytes and undetectable in E6E7-transduced and normal cervical keratinocytes. There was no significant difference in the frequency of expression of the ADAM-9 mature form (85 kDa) among the oncogenically modified cells. Modest upregulation of expression of the processed form (50 kDa) could be noticed as cells acquired viral E6E7 and progressed into tumorigenesis (fig. 3a). Similarly, cervical cancer cell lines (QG-U and Yumoto) showed significant upregulation of the processed form of ADAM-9 compared to normal cells ($p < 0.05$; fig. 3b).

Analysis of ADAM-10 revealed a band corresponding to a relative mass of approximately 85 kDa. ADAM-10 showed upregulation as keratinocytes acquire viral oncoproteins and genetic alteration(s) (fig. 3c). Densitometry analysis showed that the relative protein concentration was most prominent in the E6E7/Hras ± c-Myc-transduced keratinocytes compared to normal cervical keratinocytes ($p < 0.05$). Similarly, the level of ADAM-10 protein was upregulated in QG-U cancer cells compared to the normal cervical keratinocytes (fig. 3d).

Western blotting of ADAM-12 revealed a band corresponding to a molecular weight of about 84 kDa. Analysis showed that ADAM-12 was not expressed in normal cervical cells, but expression was noticed in E6E7 and E6E7/Hras ± c-Myc-transformed cells. Similarly, ADAM-12 protein was expressed in all the cervical cancer cell lines (fig. 3e, f).

Expression of TIMPs: The Physiological Inhibitors of ADAMs

mRNA levels of TIMP-1, -2 and -3 were analyzed by semiquantitative RT-PCR (fig. 1) and real-time PCR. Interestingly, quantitative RT-PCR showed that the transcript levels of TIMP-2 and TIMP-3, but not TIMP-1, were upregulated as cervical cells became carcinogenic compared with normal keratinocytes ($p < 0.05$; fig. 2b).

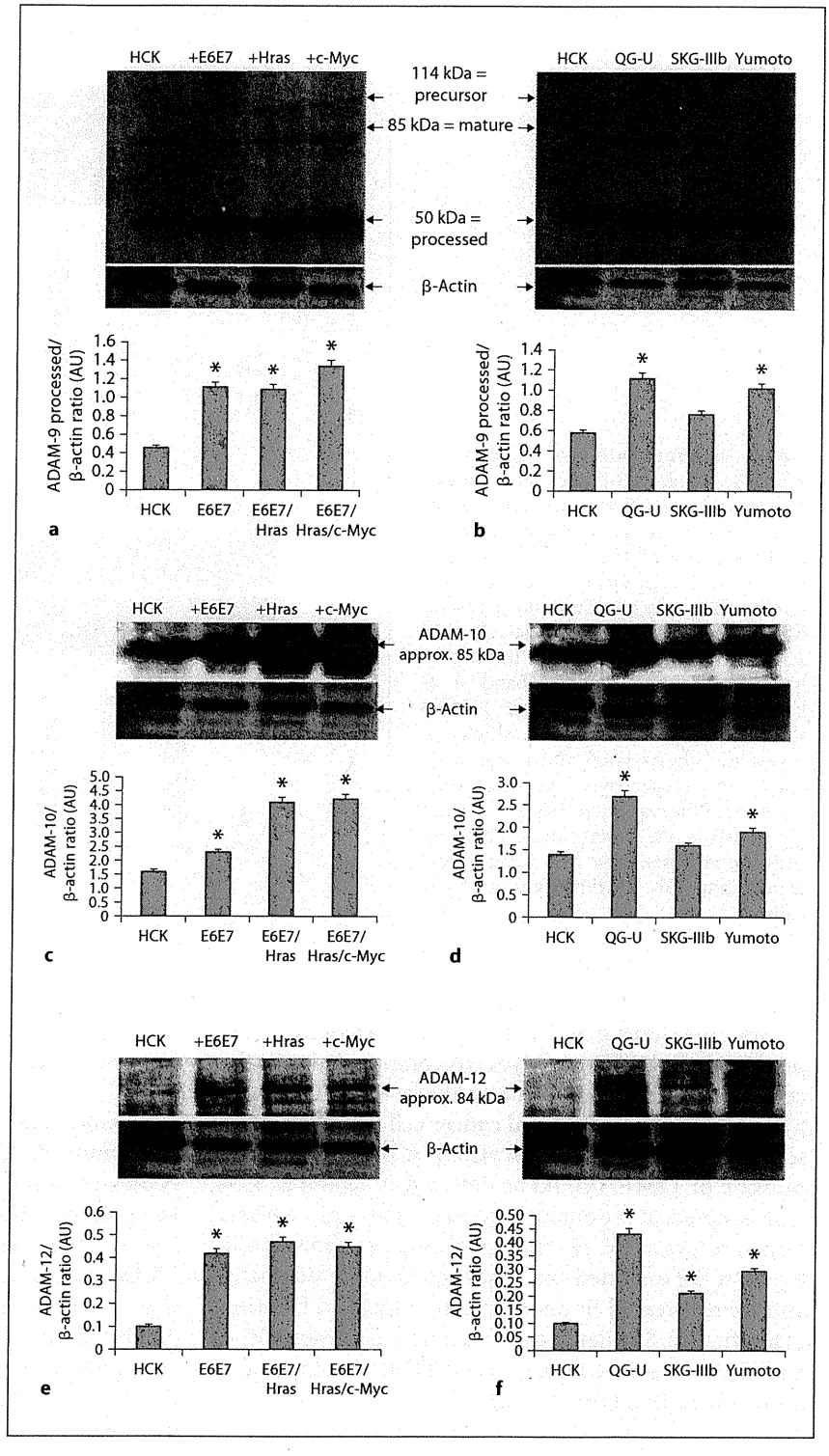

Fig. 3. Immunoblotting of ADAM-9, -10 and -12. Whole-cell lysates from normal keratinocytes (HCK = control cells), oncogenically modified keratinocytes (+E6E7 = LSILs; +Hras = HSILs; +c-Myc = invasive lesions) and 3 cervical cancer cell lines (QG-U, SKG-IIIb and Yumoto) were analyzed using specific antibodies. β-actin served as a loading control. **a**, **b** Immunoblotting of ADAM-9 shows 3 distinctive bands: precursor, mature and processed at 114, 85 and 50 kDa, respectively. **c**, **d** Immunoblotting of ADAM-10 (band at approx. 85 kDa). **e**, **f** Immunoblotting of ADAM-12 protein (band at approx. 84 kDa). The densitometric ratios of the respective ADAM to β-actin are shown in the lower panels. These results are representative of 3 independent experiments. AU = Arbitrary units. * $p < 0.05$.

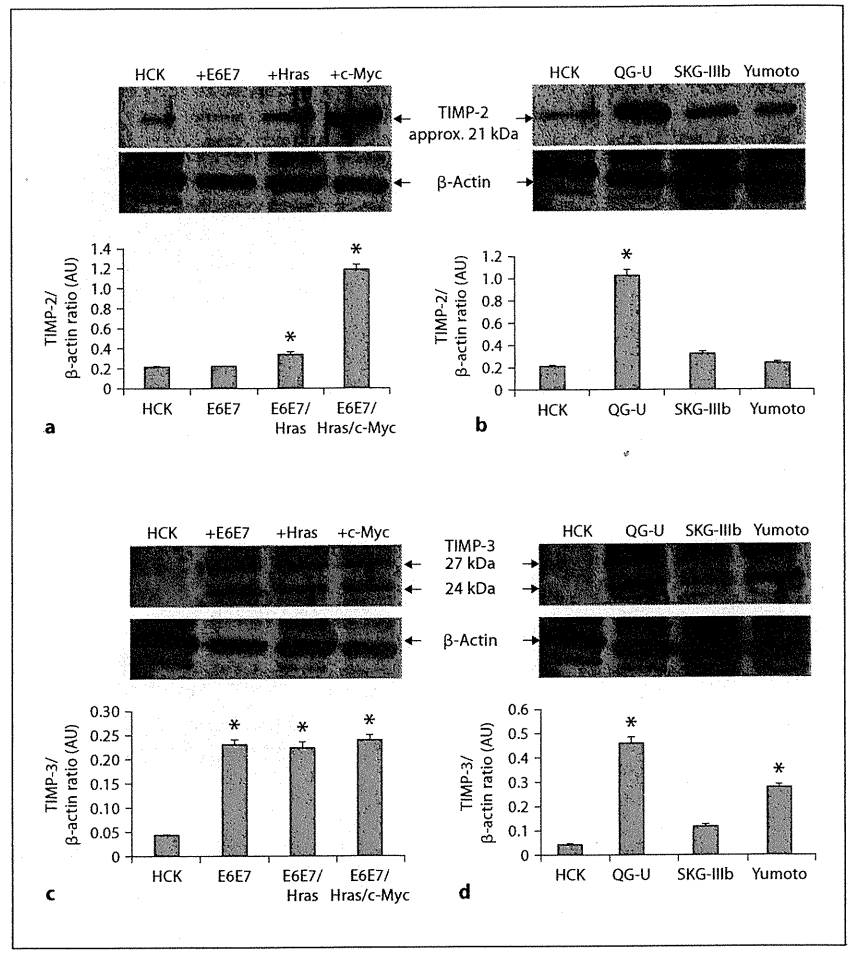

Fig. 4. Immunoblotting of TIMP-2 and TIMP-3. Whole-cell lysates from normal keratinocytes (HCK = control cells), oncogenically modified keratinocytes (+E6E7 = LSILs; +Hras = HSILs; +c-Myc = invasive lesions) and 3 cervical cancer cell lines (QG-U, SKG-IIIb and Yumoto) were analyzed using specific antibodies. β-actin served as a loading control. **a**, **b** Immunoblotting of TIMP-2 protein (band at 21 kDa). **c**, **d** Immunoblotting of TIMP-3 showed bands at 27 and 24 kDa, which represent the glycosylated and nonglycosylated forms, respectively. The densitometric ratios of the respective TIMP to β-actin are shown in the lower panels. These results are representative of 3 independent experiments. AU = Arbitrary units. * $p < 0.05$.

Immunoblotting of TIMP-2 (21 kDa) showed overexpression in E6E7/Hras/c-Myc cells compared to the other cells ($p < 0.05$; fig. 4a). Similarly, the level of TIMP-2 was higher in the QG-U cervical cancer cell line in comparison to the normal keratinocytes ($p < 0.05$; fig. 4b). Expression of TIMP-3 could be detected at 24 and 27 kDa, which represent the nonglycosylated and the glycosylated forms, respectively. Normal keratinocytes showed faint bands at the expected size that become more distinctive and overexpressed in oncogenically modified keratinocytes (fig. 4c). Similarly, cervical cancer cell lines (QG-U and Yumoto) showed upregulated TIMP-3 compared to normal keratinocytes (fig. 4d).

Immunohistochemistry

To verify the in vitro findings, we stained for ADAM-9, ADAM-10 and TIMP-3 using cervical preinvasive and invasive cervical tissues. Immunostaining was able to determine protein localization and distribution.

Immunostaining of ADAM-9

Immunostaining showed that ADAM-9 was weakly expressed in squamous epithelial cells from normal cervical tissues and localized to the superficial epithelial layers with a membranous staining pattern (fig. 5a, b). LSILs showed moderate immunostaining for ADAM-9 that involved the superficial layers in addition to the parabasal layers (fig. 5c, d). Strong immunoreactivity was noticed in most HSILs, with intense staining confined to the basal layer. In HSILs, both cytoplasmic and membranous staining was observed (fig. 5e, f). Squamous cell carcinoma revealed intense immunostaining for ADAM-9, with nuclear and cytoplasmic distribution (fig. 5g, h). Statistical tests showed that expression of

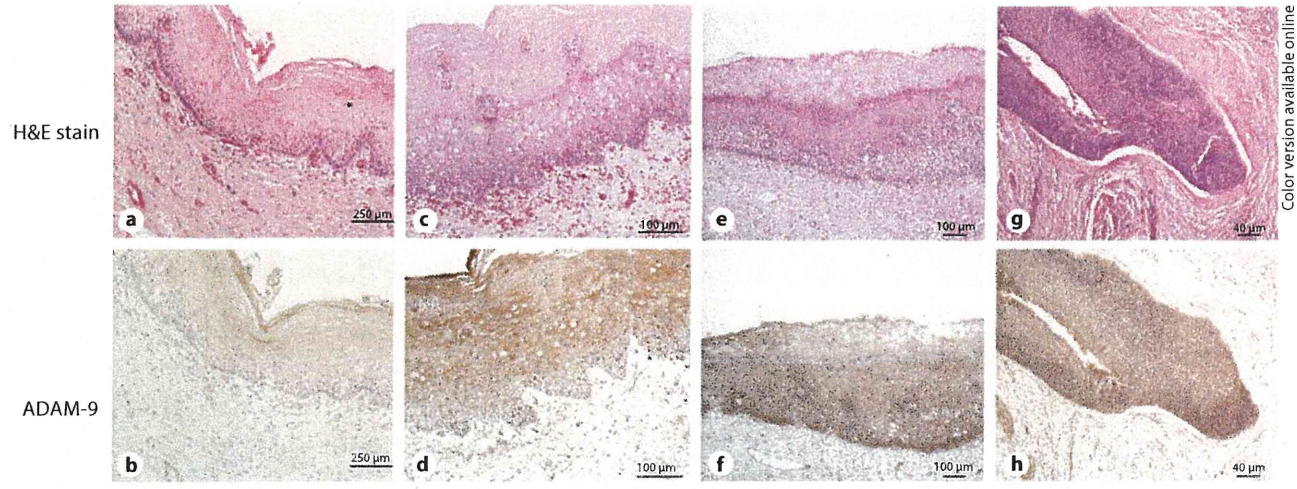

Fig. 5. Immunohistochemistry of ADAM-9 with hematoxylin (H&E) counterstaining. Expression of ADAM-9 increased with increasing severity of dysplasia in cervical squamous epithelia. **a**, **b** ADAM-9 expression is absent or weak in benign cervical epithelia. ×40. **c**, **d** In the LSIL, the expression of ADAM-9 is evident in the superficial layers with some scattering in the basal layer. ×100. **e**, **f** In the HSIL, ADAM-9 immunostaining is present in the full thickness with strong intensity in the basal layer. ×40. **g**, **h** Prominent expression of ADAM-9 is noted in the invasive cancer cells. ×100.

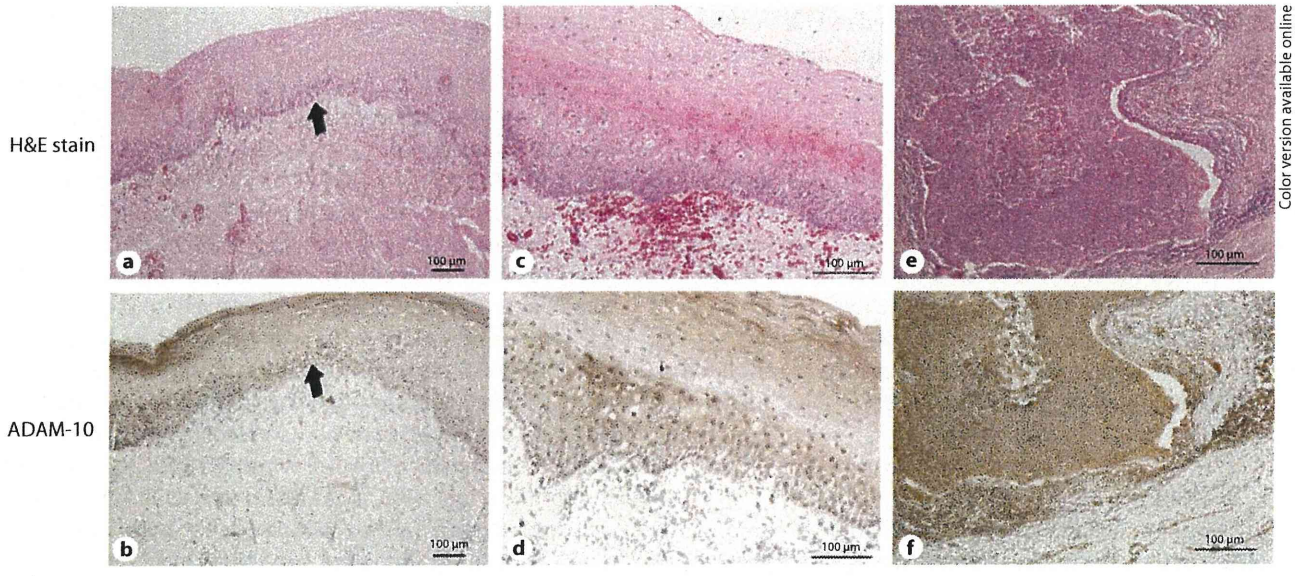

Fig. 6. Immunohistochemical detection of ADAM-10 with hematoxylin (H&E) counterstaining. **a**, **b** Note the transitional zone (arrow) between the normal epithelium (right) and the LSIL (left). ×40. ADAM-10 expression showed increased immunoreactivity as lesions became dysplastic (**b**). **c**, **d** In the LSIL, the expression of ADAM-10 is noticed in the basal and some parabasal layers. ×100. **e**, **f** Strong expression of ADAM-10 is noticed in the cancer nests in invasive cancer. ×100.

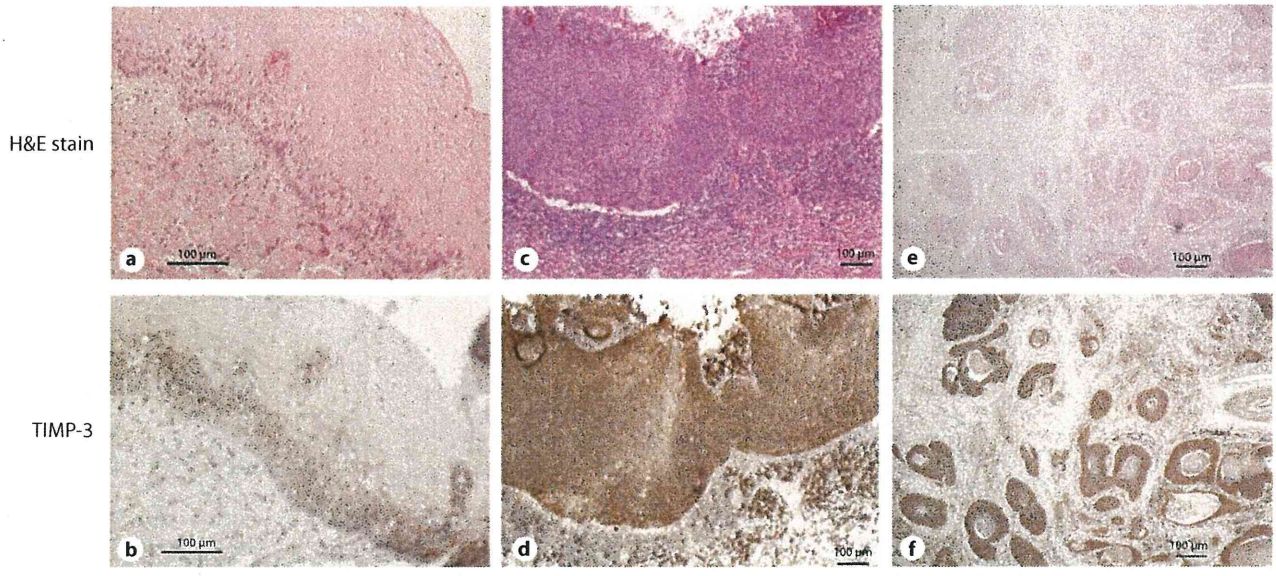

Fig. 7. Immunohistochemistry of TIMP-3 with hematoxylin (H&E) counterstaining. **a**, **b** Weak immunostaining of TIMP-3 is noted in the LSIL. ×100. **c**, **d** TIMP-3 showed moderate staining in the HSIL. ×40. **e**, **f** Strong immunoreactivity of TIMP-3 can be noted in the cancer nests in invasive cancer. ×40.

ADAM-9 is significantly upregulated in HSILs and invasive cancer compared to benign squamous epithelium ($p < 0.05$).

Immunostaining of ADAM-10

Normal cervical tissue showed absent or weak staining for ADAM-10. Dysplastic cells showed reactivity to ADAM-10 antibody (fig. 6a, b). The staining intensity of LSILs was moderate and was mainly in the basal and parabasal layers (fig. 6c, d). Invasive cancer showed strong immunostaining for ADAM-10 (fig. 6e, f). ADAM-10 expression was significantly upregulated in invasive cancer compared to the preinvasive lesions ($p < 0.05$).

Immunostaining of TIMP-3

Scattered immunoreactivity for TIMP-3 could be detected in the normal cervical mucosa. LSILs showed weak immunoreactivity confined to the basal layer (fig. 7a, b). Moderate to strong immunostaining for TIMP-3 was noticed in HSILs (fig. 7c, d), with diffuse strong immunoreactivity in invasive cancer (fig. 7e, f). TIMP-3 staining showed both nuclear and cytoplasmic patterns. Expression of TIMP-3 in squamous cell carcinoma and HSILs was significantly upregulated compared to LSILs and normal epithelium ($p < 0.05$).

Discussion

This study provides novel evidence for dysregulated expression of disintegrin proteins in squamous cell carcinoma of the uterine cervix and its precursor lesions. The mRNA level of ADAM-9, as well as the processed form of ADAM-9 protein (approx. 50 kDa), was found to be significantly upregulated when cells become oncogenically mutated compared to only virally infected cells. It was shown that a processed, alternatively spliced form of ADAM-9 is necessary for invasion through its binding to α6β4 and α2β1 integrins of colon cancer cells [30]. This work also demonstrates that the frequency and intensity of ADAM-9 expression, as assessed by immunohistochemical analysis, increases within HSILs and invasive carcinoma relative to LSILs and normal cells. Our immunohistochemical data are in accordance with a previous report indicating increased ADAM-9 immunoreactivity in both cervical intraepithelial neoplasia grade 3 (CIN3) and invasive tumors of the uterine cervix [31]. Physiologically, it was shown that mouse ADAM-9 is not essential for normal development or adult homeostasis [32]. However, human ADAM-9 was found to regulate keratinocyte migration through interaction with β1 integrins and modulation of MMP synthesis [33]. The expression of ADAM-9 was previously reported to be upregulated at

the mRNA and/or protein level in various solid cancers [34–36]. Furthermore, ADAM-9 overexpression in lung tumor is correlated with brain metastasis [37]. Hence, the biological role of ADAM-9 in cancer could relate to its ability to bind integrins and to degrade extracellular matrix, which promote cell invasion [30]. In addition, blocking ADAM-9 in gastric cancer resulted in inhibition of cell growth of gastric cancer cell lines [38].

Our study describes, for the first time, the expression and regulation of ADAM-10 during cervical carcinogenesis. ADAM-10 was upregulated in oncogenically mutated keratinocytes compared to normal or virally infected cells. The result was confirmed by examining the immunoreactivity of ADAM-10 in preinvasive and invasive cervical tissues. It was found that ADAM-10 could cleave several extracellular matrix components, such as collagen IV of the basement membrane [39], and can also increase the motility of keratinocytes through its ability to shed soluble basement membrane collagen XVII (BPAG2), which supports interactions between the basal cells and the underlying basement membrane [40]. Aberrant expression of collagen XVII in invasive cervical lesions has been investigated elsewhere [41]. However, the relationship between collagen XVII and ADAM-10 in cervical lesions requires further study. Overexpression of ADAM-10 was also found in prostate and oral cancers [42, 43].

This work describes the novel expression of ADAM-12 in cervical carcinogenesis. Interestingly, normal keratinocytes did not express ADAM-12, while virally infected and oncogenically modified keratinocytes showed ADAM-12 expression. As shown by quantitative RT-PCR, the long form of ADAM-12, but not the short form, was only found to be upregulated during cervical carcinogenesis. This finding is similar to the expression of ADAM-12 in lung and bladder cancers [44, 45]. Experimental studies showed that the ADAM-12 level is associated with cancer through degradation of extracellular matrix, as well as regulation of cell proliferation and apoptosis [46, 47]. Earlier studies showed that the cytoplasmic parts of ADAM-12 and ADAM-15 interact with Src homology 3 domain to exert their actions [48, 49].

Taking these findings together, we can conclude that the upregulation of ADAM-12 by invasive cervical cells, compared to absent expression in normal cells, plays an important role in the steps of cervical carcinogenesis.

TIMPs, endogenous regulators of MMPs, can selectively inhibit several ADAMs and ADAMTSs [48]. Therefore, TIMPs can regulate the degradation of extracellular matrix and control cell ligand shedding. Immunoblotting assays showed upregulation of TIMP-2 and TIMP-3 during the course of cervical carcinogenesis, with the highest expression in the invasive phenotype. Biologically, TIMP-2 can selectively inhibit ADAM-12, while TIMP-3 has a wide range of inhibitory effects against ADAMs, including ADAM-10 and ADAM-12 [50, 51].

The expression of TIMPs, in relation to ADAMs, was reported to be dysregulated during several pathological conditions [52]. The aberrant expression of TIMP-2 and -3 in cervical lesions might be biologically relevant, but not exclusively, to the activities of the investigated ADAMs. Based on quantitative RT-PCR results, the selected ADAMTS members might have no role during cervical neoplasia, such as ADAMs do.

In summary, the dysregulated expression of several ADAMs during cervical carcinogenesis can be best noticed when cervical cells acquire genetic alteration(s), as infection with HPV alone, as seen in LSILs, is not enough to provoke ADAM expression significantly. However, synergistic effects of viral oncoproteins and genetic change(s) cannot be ruled out. We can conclude that the expression of several ADAMs, as well as their endogenous regulators, is dysregulated in cervical neoplasia. ADAM-9, -10 and -12 are overexpressed in HSILs and cancerous cells, suggesting that these proteins could play a crucial role in the pathogenesis of cervical carcinoma. The exact mechanism of action requires further studies to determine the biological effects of these proteins during the cascades of cervical neoplasia.

References

1 Thun MJ, DeLancey JO, Center MM, Jemal A, Ward EM: The global burden of cancer: priorities for prevention. Carcinogenesis 2010;31:100–110.

2 Stoler MH: Human papillomaviruses and cervical neoplasia: a model for carcinogenesis. Int J Gynecol Pathol 2000;19:16–28.

3 Münger K, Baldwin A, Edwards KM, Hayakawa H, Nguyen CL, Owens M, Grace M, Huh K: Mechanisms of human papillomavirus-induced oncogenesis. J Virol 2004;78:11451–11460.

4 zur Hausen H: Papillomaviruses and cancer: from basic studies to clinical application. Nat Rev Cancer 2002;2:342–350.

5 Wolfsberg TG, Primakoff P, Myles DG, White JM: ADAM, a novel family of membrane proteins containing A Disintegrin And Metalloprotease domain: multipotential functions in cell-cell and cell-matrix interactions. J Cell Biol 1995;131:275–278.

6 Jones GC, Riley GP: ADAMTS proteinases: a multi-domain, multi-functional family with roles in extracellular matrix turnover and arthritis. Arthritis Res Ther 2005;7:160–169.
7 Van Goor H, Melenhorst WB, Turner AJ, Holgate ST: Adamalysins in biology and disease. J Pathol 2009;219:277–286.
8 Higuchi Y, Yasui A, Matsuura K, Yamamoto S: CD156 transgenic mice. Different responses between inflammatory types. Pathobiology 2002;70:47–54.
9 Shiomi T, Lemaître V, D'Armiento J, Okada Y: Matrix metalloproteinases, a disintegrin and metalloproteinases, and a disintegrin and metalloproteinases with thrombospondin motifs in non-neoplastic diseases. Pathol Int 2010;60:477–496.
10 Eto K, Huet C, Tarui T, Kupriyanov S, Liu HZ, Puzon-McLaughlin W, Zhang XP, Sheppard D, Engvall E, Takada Y: Functional classification of ADAMs based on a conserved motif for binding to integrin alpha 9 beta1: implications for sperm-egg binding and other cell interactions. J Biol Chem 2002; 277:17804–17810.
11 Yang P, Baker KA, Hagg T: The ADAMs family: coordinators of nervous system development, plasticity and repair. Prog Neurobiol 2006;79:73–94.
12 Gilpin BJ, Loechel F, Mattei MG, Engvall E, Albrechtsen R, Wewer UM: A novel, secreted form of human ADAM 12 (meltrin alpha) provokes myogenesis in vivo. J Biol Chem 1998;273:157–166.
13 Kawaguchi N, Xu X, Tajima R, Kronqvist P, Sundberg C, Loechel F, Albrechtsen R, Wewer UM: ADAM 12 protease induces adipogenesis in transgenic mice. Am J Pathol 2002;160:1895–1903.
14 Duffy MJ, McKiernan E, O'Donovan N, McGowan PM: Role of ADAMs in cancer formation and progression. Clin Cancer Res 2009;15:1140–1144.
15 Mochizuki S, Okada Y: ADAMs in cancer cell proliferation and progression. Cancer Sci 2007;98:621–628.
16 Apte SS: A disintegrin-like and metalloprotease (reprolysin-type) with thrombospondin type 1 motif (ADAMTS) superfamily: functions and mechanisms. J Biol Chem 2009;284:31493–31497.
17 Liu YJ, Xu Y, Yu Q: Full-length ADAMTS-1 and the ADAMTS-1 fragments display pro- and antimetastatic activity, respectively. Oncogene 2006;25:2452–2467.
18 Rocks N, Paulissen G, El Hour M, Quesada F, Crahay C, Gueders M, Foidart JM, Noel A, Cataldo D: Emerging roles of ADAM and ADAMTS metalloproteinases in cancer. Biochimie 2008;90:369–379.
19 Murphy G: The ADAMs: signalling scissors in the tumour microenvironment. Nat Rev Cancer 2008;8:929–941.
20 Maskos K, Fernandez-Catalan C, Huber R, Bourenkov GP, Bartunik H, Ellestad GA, Reddy P, Wolfson MF, Rauch CT, Castner BJ, Davis R, Clarke HR, Petersen M, Fitzner JN, Cerretti DP, March CJ, Paxton RJ, Black RA, Bode W: Crystal structure of the catalytic domain of human tumor necrosis factor-alpha-converting enzyme. Proc Natl Acad Sci USA 1998;95:3408–3412.
21 Brew K, Dinakarpandian D, Nagase H: Tissue inhibitors of metalloproteinases: evolution, structure and function. Biochim Biophys Acta 2000;1477:267–283.
22 Amour A, Knight CG, Webster A, Slocombe PM, Stephens PE, Knäuper V, Docherty AJ, Murphy G: The in vitro activity of ADAM-10 is inhibited by TIMP-1 and TIMP-3. FEBS Lett 2000;473:275–279.
23 Kashiwagi M, Tortorella M, Nagase H, Brew K: TIMP-3 is a potent inhibitor of aggrecanase 1 (ADAM-TS4) and aggrecanase 2 (ADAM-TS5). J Biol Chem 2001;276:12501–12504.
24 Hanahan D, Weinberg RA: The hallmarks of cancer. Cell 2000;100:57–70.
25 Sheu BC, Lien HC, Ho HN, Lin HH, Chow SN, Huang SC, Hsu SM: Increased expression and activation of gelatinolytic matrix metalloproteinases is associated with the progression and recurrence of human cervical cancer. Cancer Res 2003;63:6537–6542.
26 Libra M, Scalisi A, Vella N, Clementi S, Sorio R, Stivala F, Spandidos DA, Mazzarino C: Uterine cervical carcinoma: role of matrix metalloproteinases. Int J Oncol 2009;34: 897–903.
27 Ueda M, Terai Y, Yamashita Y, Kumagai K, Ueki K, Yamaguchi H, Akise D, Hung YC, Ueki M: Correlation between vascular endothelial growth factor-C expression and invasion phenotype in cervical carcinomas. Int J Cancer 2002;98:335–343.
28 Mitsuhashi A, Tanaka H, Tanaka N, Sugita M, Shirasawa H, Tokita H, Eda H, Sekiya S: Establishment and characterization of a new HPV-negative squamous cell carcinoma cell line (Yumoto) from the human uterine cervix. Gynecol Oncol 1998;70:339–347.
29 Narisawa-Saito M, Yoshimatsu Y, Ohno S, Yugawa T, Egawa N, Fujita M, Hirohashi S, Kiyono T: An in vitro multistep carcinogenesis model for human cervical cancer. Cancer Res 2008;68:5699–5705.
30 Mazzocca A, Coppari R, De Franco R, Cho JY, Libermann TA, Pinzani M, Toker A: A secreted form of ADAM9 promotes carcinoma invasion through tumor-stromal interactions. Cancer Res 2005;65:4728–4738.
31 Zubel A, Flechtenmacher C, Edler L, Alonso A: Expression of ADAM9 in CIN3 lesions and squamous cell carcinomas of the cervix. Gynecol Oncol 2009;114:332–336.
32 Weskamp G, Cai H, Brodie TA, Higashyama S, Manova K, Ludwig T, Blobel CP: Mice lacking the metalloprotease-disintegrin MDC9 (ADAM9) have no evident major abnormalities during development or adult life. Mol Cell Biol 2002;22:1537–1544.
33 Zigrino P, Steiger J, Fox JW, Löffek S, Schild A, Nischt R, Mauch C: Role of ADAM-9 disintegrin-cysteine-rich domains in human keratinocyte migration. J Biol Chem 2007; 282:30785–30793.
34 O'Shea C, McKie N, Buggy Y, Duggan C, Hill AD, McDermott E, O'Higgins N, Duffy MJ: Expression of ADAM-9 mRNA and protein in human breast cancer. Int J Cancer 2003; 105:754–761.
35 Zigrino P, Mauch C, Fox JW, Nischt R: Adam-9 expression and regulation in human skin melanoma and melanoma cell lines. Int J Cancer 2005;116:853–859.
36 Peduto L, Reuter VE, Shaffer DR, Scher HI, Blobel CP: Critical function for ADAM9 in mouse prostate cancer. Cancer Res 2005;65: 9312–9319.
37 Shintani Y, Higashiyama S, Ohta M, Hirabayashi H, Yamamoto S, Yoshimasu T, Matsuda H, Matsuura N: Overexpression of ADAM9 in non-small cell lung cancer correlates with brain metastasis. Cancer Res 2004;64:4190–4196.
38 Carl-McGrath S, Lendeckel U, Ebert M, Roessner A, Rocken C: The disintegrin-metalloproteinases ADAM9, ADAM12, and ADAM15 are upregulated in gastric cancer. Int J Oncol 2005;26:17–24.
39 Millichip M, Dallas D, Wu E, Dale S, McKie N: The metallo-disintegrin ADAM10 (MADM) from bovine kidney has type IV collagenase activity in vitro. Biochem Biophys Res Commun 1998;245:594–598.
40 Franzke CW, Tasanen K, Schacke H, Zhou Z, Tryggvason K, Mauch C, Zigrino P, Sunnarborg S, Lee DC, Fahrenholz F, Bruckner-Tuderman L: Transmembrane collagen XVII, an epithelial adhesion protein, is shed from the cell surface by ADAMs. EMBO J 2002;21: 5026–5035.
41 Yamada T, Endo R, Tsukagoshi K, Fujita S, Honda K, Kinoshita M, Hasebe T, Hirohashi S: Aberrant expression of a hemidesmosomal protein, bullous pemphigoid antigen 2, in human squamous cell carcinoma. Lab Invest 1996;75:589–600.
42 McCulloch DR, Akl P, Samaratunga H, Herington AC, Odorico DM: Expression of the disintegrin metalloprotease, ADAM-10, in prostate cancer and its regulation by dihydrotestosterone, insulin-like growth factor I, and epidermal growth factor in the prostate cancer cell model LNCaP. Clin Cancer Res 2004;10:314–323.
43 Ko SY, Lin SC, Wong YK, Liu CJ, Chang KW, Liu TY: Increase of disintergin metalloprotease 10 (ADAM10) expression in oral squamous cell carcinoma. Cancer Lett 2007;245: 33–43.

44 Rocks N, Paulissen G, Quesada Calvo F, Polette M, Gueders M, Munaut C, Foidart JM, Noel A, Birembaut P, Cataldo D: Expression of a disintegrin and metalloprotease (ADAM and ADAMTS) enzymes in human non-small-cell lung carcinomas (NSCLC). Br J Cancer 2006;94:724–730.
45 Fröhlich C, Albrechtsen R, Dyrskjøt L, Rudkjaer L, Ørntoft TF, Wewer UM: Molecular profiling of ADAM12 in human bladder cancer. Clin Cancer Res 2006;12:7359–7368.
46 Roy R, Wewer UM, Zurakowski D, Pories SE, Moses MA: ADAM 12 cleaves extracellular matrix proteins and correlates with cancer status and stage. J Biol Chem 2004;279:51323–51330.
47 Rocks N, Estrella C, Paulissen G, Quesada-Calvo F, Gilles C, Guéders MM, Crahay C, Foidart JM, Gosset P, Noel A, Cataldo DD: The metalloproteinase ADAM-12 regulates bronchial epithelial cell proliferation and apoptosis. Cell Prolif 2008;41:988–1001.
48 Mori S, Tanaka M, Nanba D, Nishiwaki E, Ishiguro H, Higashiyama S, Matsuura N: PACSIN3 binds ADAM12/meltrin alpha and up-regulates ectodomain shedding of heparin-binding epidermal growth factor-like growth factor. J Biol Chem 2003;278:46029–46034.
49 Yasui A, Matsuura K, Shimizu E, Hijiya N, Higuchi Y, Yamamoto S: Expression of splice variants of the human ADAM15 gene and strong interaction between the cytoplasmic domain of one variant and Src family proteins Lck and Hck. Pathobiology 2004;71:185–192.
50 Edwards DR, Handsley MM, Pennington CJ: The ADAM metalloproteinases. Mol Aspects Med 2008;29:258–289.
51 Kveiborg M, Jacobsen J, Lee MH, Nagase H, Wewer UM, Murphy G: Selective inhibition of ADAM12 catalytic activity through engineering of tissue inhibitor of metalloproteinase 2 (TIMP-2). Biochem J 2010;430:79–86.
52 Fedak PW, Moravec CS, McCarthy PM, Altamentova SM, Wong AP, Skrtic M, Verma S, Weisel RD, Li RK: Altered expression of disintegrin metalloproteinases and their inhibitor in human dilated cardiomyopathy. Circulation 2006;113:238–245.

NEOPLASIA
www.neoplasia.com

Volume 13 Number 9 September 2011 pp. 864–873 **864**

NRF2 Mutation Confers Malignant Potential and Resistance to Chemoradiation Therapy in Advanced Esophageal Squamous Cancer[1]

Tatsuhiro Shibata*,†, Akiko Kokubu*, Shigeru Saito‡, Mako Narisawa-Saito§, Hiroki Sasaki¶, Kazuhiko Aoyagi¶, Yuki Yoshimatsu§, Yuji Tachimori#, Ryoji Kushima†, Tohru Kiyono§ and Masayuki Yamamoto**

*Division of Cancer Genomics, National Cancer Center Research Institute, Tokyo, Japan; †Pathology and Clinical Laboratory Division, National Cancer Center Hospital, Tokyo, Japan; ‡Chem and Bio Informatics Department, Infocom Corporation, Tokyo, Japan; §Division of Virology, National Cancer Center Research Institute, Tokyo, Japan; ¶Division of Integrative Omics and Bioinformatics, National Cancer Center Research Institute, Tokyo, Japan; #Gastrointestinal Oncology Division, National Cancer Center Hospital, Tokyo, Japan; **Department of Medical Biochemistry, Tohoku University Graduate School of Medicine, Sendai, Japan

Abstract

Esophageal squamous cancer (ESC) is one of the most aggressive tumors of the gastrointestinal tract. A combination of chemotherapy and radiation therapy (CRT) has improved the clinical outcome, but the molecular background determining the effectiveness of therapy remains unknown. NRF2 is a master transcriptional regulator of stress adaptation, and gain-of-function mutation of NRF2 in cancer confers resistance to stressors including anticancer therapy. Direct resequencing analysis revealed that *Nrf2* gain-of-function mutation occurred recurrently (18/82, 22%) in advanced ESC tumors and ESC cell lines (3/10). The presence of *Nrf2* mutation was associated with tumor recurrence and poor prognosis. Short hairpin RNA–mediated down-regulation of NRF2 in ESC cells that harbor only mutated *Nrf2* allele revealed that the mutant NRF2 conferred increased cell proliferation, attachment-independent survival, and resistance to 5-fluorouracil and γ-irradiation. Based on the *Nrf2* mutation status, gene expression signatures associated with *NRF2* mutation were extracted from ESC cell lines, and their potential utility for monitoring and prognosis was examined in a cohort of 33 pre-CRT cases of ESC. The molecular signatures of *NRF2* mutation were significantly predictive and prognostic for CRT response. In conclusion, recurrent *NRF2* mutation confers malignant potential and resistance to therapy in advanced ESC, resulting in a poorer outcome. Molecular signatures of *NRF2* mutation can be applied as predictive markers of response to CRT, and efficient inhibition of aberrant NRF2 activation could be a promising approach in combination with CRT.

Neoplasia (2011) 13, 864–873

Introduction

Esophageal cancer (EC) is the sixth most common cause of cancer death worldwide [1]. The 5-year survival rate of patients with EC is reportedly less than 20%, making it one of the most aggressive tumors of the gastrointestinal tract [2]. Epidemiologically, alcohol consumption, cigarette smoking, and a preference for hot beverages, as well as the presence of Barrett esophagus resulting from gastroesophageal reflux, have been reported as risk factors for EC [3,4], and more than

Address all correspondence to: Tatsuhiro Shibata, MD, PhD, Cancer Genomics Project, National Cancer Center Research Institute, 5-1-1, Tsukiji, Chuo-ku, Tokyo, 104-0045, Japan. E-mail: tashibat@ncc.go.jp

[1]This study was supported in part by a Grant-in-Aid for the Comprehensive 10-Year Strategy for Cancer Control, the Grant-in-Aid for Cancer Research (19-1) from the Ministry of Health, Labor and Welfare, Japan and Research Grant of the Princess Takamatsu Cancer Research Fund 08-24007. The authors declare no conflicts of interest.
[2]This article refers to supplementary materials, which are designated by Tables W1 to W3 and Figures W1 to W4 and are available online at www.neoplasia.com.
Received 23 May 2011; Revised 24 June 2011; Accepted 27 June 2011

DOI 10.1593/neo.11750

460,000 patients develop this cancer annually worldwide [1]. Esophageal squamous cancer (ESC) is the predominant type of EC, being prevalent in Africa and Eastern Asia including Japan [5].

Currently, only surgical resection can be regarded as a curative therapy for ESC, and adjuvant or neoadjuvant combination of chemotherapy with radiation therapy (CRT) has recently improved the clinical outcome [6–8]. However, responsiveness to CRT varies among patients, and the molecular backgrounds that determine therapeutic effectiveness remain largely unknown [6]. Therefore, the discovery of molecular markers for precise prediction of responsiveness to therapy is eagerly anticipated. It is also necessary to construct effective personalized therapeutic modalities based on the molecular characterization of ESC.

Oxidative stress has been shown to play important roles in the carcinogenesis and progression of many cancers including ESC [9–11]. In response to intrinsic (e.g., reactive oxygen species generated in mitochondria) and extrinsic (e.g., radiation) oxidative stresses, NEF2L2 (nuclear erythroid factor 2-like 2, or NRF2) functions as a master transcriptional regulator of cytoprotective genes [12]. Under physiological conditions, KEAP1, an E3 ubiquitin ligase, directly interacts with two amino-terminal motifs (DLG and ETGE) of NRF2 and negatively regulates its expression level through the proteasome [13]. Recently, it has been revealed that aberrant activation of the NRF2 pathway occurs frequently in cancer. We and other groups have reported that the *Keap1* gene is inactivated in a wide range of cancers [14–18]. Moreover, we have discovered that the *Nrf2* gene is a *bona fide* oncogene in lung and head/neck cancers [19]. In the present study, we discovered that *NRF2* mutation also occurs frequently in ESC and examined its clinical significance especially from the viewpoint of responsiveness to CRT.

Materials and Methods

Clinical Samples and DNA Extraction

All surgical specimens were obtained from patients who had been diagnosed and had undergone surgery at the National Cancer Center Hospital, Tokyo, Japan (pathologic diagnoses are presented in Table W1). Tumor cells and corresponding lymphocytes or noncancerous tissues were dissected under a microscope from methanol-fixed or formalin-fixed (*in situ* carcinoma) paraffin-embedded tissues, and the DNA was extracted. High-molecular-weight DNA was also extracted from cell lines using DNAeasy (QIAGEN, Hamburg, Germany). Clinical data, including therapeutic response and prognosis, were collected from the medical charts. The protocol for analysis of the clinical samples was approved by the institutional review board of the National Cancer Center.

Polymerase Chain Reaction and Sequence Analysis

We amplified all exons of the Nrf2 gene by polymerase chain reaction (PCR) using High-Fidelity Taq polymerase (Roche Diagnostic, Basel, Switzerland), as described [19]. The PCR products were then purified (QIAquick PCR Purification Kit; QIAGEN) and analyzed by sequencing (Big Dye Sequencing Kit; Applied Biosystems, Carlsbad, CA).

Biologic and Biochemical Experiments

Ten ESC cell lines (KYSE-30, -50, -70, -110, -140, -150, -170, -180, -220, and -270) were obtained from the Japanese Collection of Research Bioresources (http://cellbank.nibio.go.jp) and maintained in Dulbecco modified Eagle medium supplemented with 10% fetal bovine serum. Construction of the retroviral expression vector of short hairpin RNA (shRNA) was carried out as described previously [20]. The shRNA-targeted sequences were as follows: NRF2–shRNA-1, ACTTGCTCAATGTCCTGTTGC; NRF2–shRNA-2, AGTTGAGCTTCATTGAACTGC. The control vector contains nontargeting shRNA sequence. The entry vectors were recombined with pDEST-CL-SI-MSCVpuro by LR reactions (Invitrogen, Carlsbad, CA), in accordance with the manufacturer's instructions. After infection (multiplicity of infection > 1), cells were selected and maintained in the presence of 1 μg/ml puromycin. NRF2 small interfering RNA (siRNA) was previously described [19]. NRF2-dependent luciferase activity was measured as described [15]. Cell proliferation was measured using the 96-well plate format by bromodeoxyuridine incorporation (Cell Proliferation ELISA; Roche Diagnostic). For attachment-free culture, 1×10^6 cells were seeded in ultra low-attachment dish (Ultra Low Cluster Plate, Corning, NY). 5-Fluorouracil (5-FU) was purchased from WAKO (Tokyo). Irradiation of cells was performed using the ^{60}Co source in the Gammacell 220 Research Irradiator (MDS Nordion, Ontario, Canada). The intracellular level of reduced glutathione was measured by GSH-Glo Glutathione Assay (Promega, Madison, WI). Protein extraction and immunoblot analysis were performed as described previously [15]. Antibodies used in this study are listed in Table W1.

Gene Expression Profiling and Quantitative Reverse Transcription–PCR

Ten micrograms of total RNA from ESC cell lines was reverse-transcribed by MMLV-RT, and a Cy3-labeled complementary RNA probe was synthesized using T7 RNA polymerase and hybridized with a microarray covering the whole human genome (Whole Human Genome Oligo Microarray, G4112F; Agilent Technologies, Santa Clara, CA). After washing, the microarray was scanned by the DNA microarray scanner (Agilent Technologies). Data were analyzed using GeneSpring software (Agilent Technologies). Quantitative reverse transcription (RT)–PCR was performed in triplicate and evaluated using universal probes for each amplicon and the LightCycler system (Roche). Primers designed by ProbeFinder (Version 2.45; Roche) and used in this study are shown in Table W2. The relative expression of each gene was determined by comparison with that of glyceraldehyde-3-phosphate dehydrogenase (GADPH).

Statistics

Statistical analysis of clinicopathologic data was performed using the StatView software package. Gene Set Enrichment Analysis (GSEA) was performed as follows. First, a gene list sorted in descending order based on fold change differences in expression between *NRF2*-mutated and wild-type ESC cell lines was calculated. Second, preranked GSEA was applied for the gene list to the C2 curated gene sets (MSigDB ver. 2.5) with default parameters (http://www.broadinstitute.org/gsea/index.jsp). Finally, significant gene sets were extracted if the false discovery rate (FDR) was less than 25%. To evaluate the predictive power of gene expression signatures for CRT and prognosis, biopsy samples with clinical information were classified into two groups by K-means clustering (R cluster package) using gene expression signatures for each significant gene set of GSEA, and then survival analysis was applied to the classified samples. The survival analysis was performed using the Kaplan-Meier method, and log-rank test was used to evaluate disease-free survival. To determine whether the NRF2 target genes based on ChIP-seq (chromatin immunoprecipitation sequence) [21] were enriched in any gene sets, we calculated the *P* values using the hypergeometric distribution for each the C2 curated gene sets and estimated the FDR.

Because the NRF2 ChIP-seq data were measured using a mouse cell line, we then converted the mouse genes to human genes using NCBI HomoloGene to apply them as a human gene set C2. We used a 10% FDR cutoff for this enrichment study.

Results

NRF2 *Mutation in ESC*

To evaluate the prevalence of *NRF2* mutation in human cancer, we attempted resequencing analysis of the entire coding region of the *NRF2* gene in a cohort (320 samples in total) of epithelial and nonepithelial tumors (pathologic diagnoses are shown in Table W2). We detected six nonsynonymous somatic mutations in the ECs (6/32, 18.8%) and one nonsynonymous somatic mutation in cervical cancer (1/18, 5.6%) and malignant melanoma (1/22, 4.5%), respectively (Figure 1*A* and Table 1). We additionally analyzed 50 cases of ESC and identified a total of 18 somatic mutations (18/82, 22%; Table 1). These mutations exclusively affected amino acid residues within and surrounding the KEAP1 binding motif, as reported previously in lung cancers [19]. We then analyzed 10 ESC cell lines and found three *NRF2*-mutated ones (3/10; Figure 1*B* and Table 1), of which two (KYSE70 and KYSE180) harbored homozygous mutations. *NRF2*-mutated KYSE70 and KYSE110 cells were established from poorly differentiated ESC. No *KEAP1* mutation was detected in ESC cases (data not shown). We additionally analyzed 36 cases of intraepithelial (*in situ*) ESC and detected no *NRF2* mutation (0/36), suggesting that *NRF2* mutation occurs predominantly at the advanced stage of esophageal carcinogenesis.

Association of NRF2 *Mutation with Tumor Recurrence and Poor Prognosis of ESC*

To further determine the clinical significance of *NRF2* gene mutation in EC, we analyzed the association between *NRF2* mutation status and clinicopathologic factors. The presence of *NRF2* mutation was correlated with tumor recurrence ($P = .046$) and tended to be associated with lymph node metastasis ($P = .072$). Patients with *NRF2*-mutated tumors showed poorer survival ($P = .005$; Table 2 and Figure 1*C*). Clinical stage ($P = .038$) and lymph node metastasis ($P = .039$) were associated with the disease-free survival of the patient (Table 2).

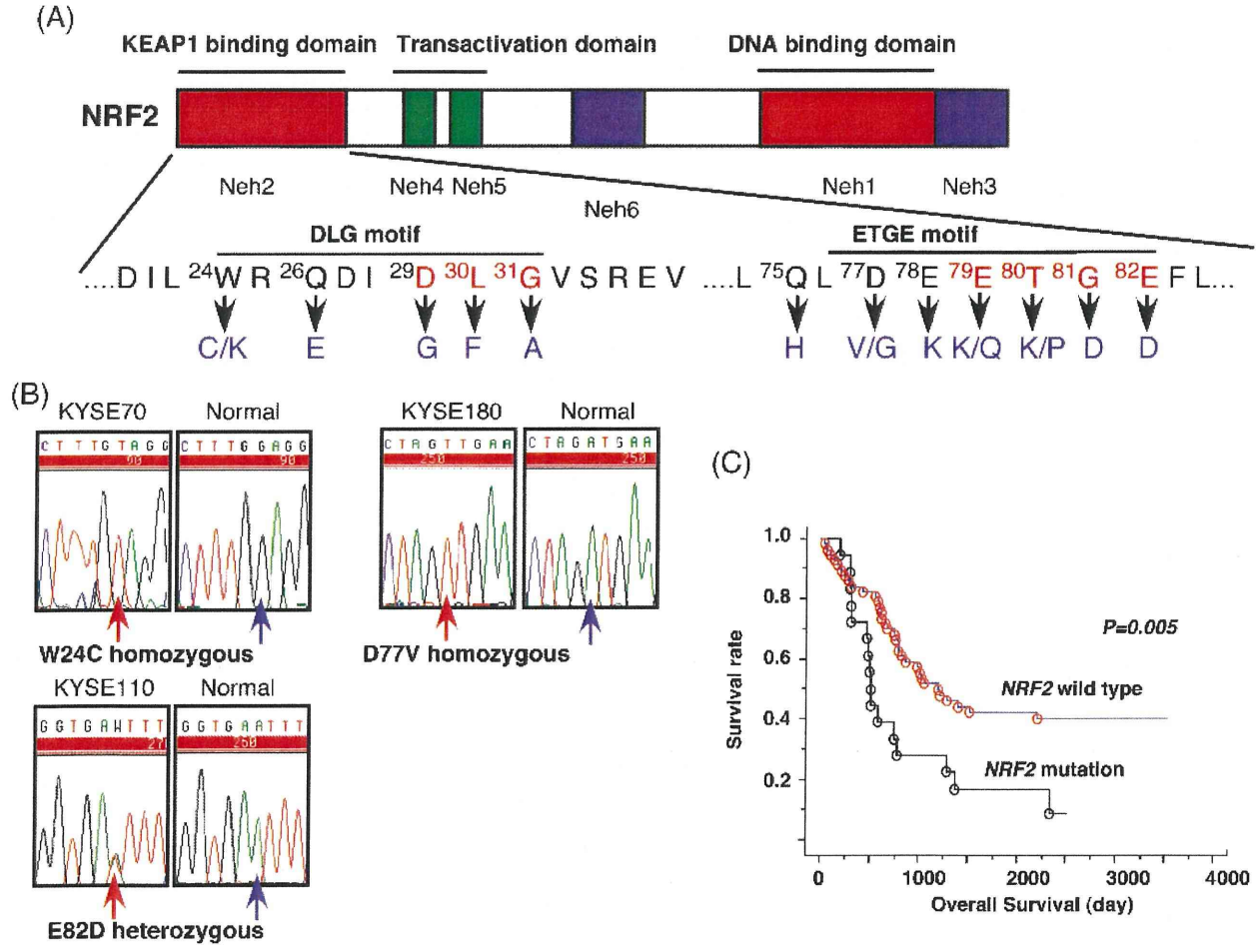

Figure 1. *NRF2* mutation in EC. (A) Somatic NRF2 mutations are clustered in the KEAP1 binding domain. Schematic presentation of NRF2 protein indicates the location of Neh1~6 (Nrf2-ech homology) domains and functional annotations. Somatic mutations identified in this study (blue) affected amino acids in the DLG or ETGE motifs. (B) Sequence chromatography of NRF2 mutations in ESC cell lines with corresponding normal sequences in the bottom panel. KYSE70 and KYSE180 cells harbor homozygous mutations. (C) Kaplan-Meier plot showing overall survival of ESC patients segregated according to NRF2 mutation status.

Table 1. *NRF2* Mutation in Human Cancers.

Sex	Tumor Type	Nucleotide Substitution	Amino Acid Change	Zygosity
M	Esophageal cancer (SCC)	c. 70T>C	p. W24K	Heterozygous
F	Esophageal cancer (SCC)	c. 72G>C	p. W24C	Heterozygous
M	Esophageal cancer (SCC)	c. 76C>G	p. Q26E	Heterozygous
M	Esophageal cancer (SCC)	c. 66A>G	p. D29G	Heterozygous
M	Esophageal cancer (SCC)	c. 66A>G	p. D29G	Allelic imbalance (mut > wt)
M	Esophageal cancer (SCC)	c. 88C>T	p. L30F	Heterozygous
M	Esophageal cancer (SCC)	c. 92G>C	p. G31A	Heterozygous
M	Esophageal cancer (SCC)	c. 225A>C	p. Q75H	Heterozygous
M	Esophageal cancer (SCC)	c. 230A>T	p. D77V	Heterozygous
M	Esophageal cancer (SCC)	c. 230A>G	p. D77G	Heterozygous
M	Esophageal cancer (SCC)	c. 232G>A	p. E78K	Heterozygous
M	Esophageal cancer (SCC)	c. 235G>A	p. E79K	Heterozygous
M	Esophageal cancer (SCC)	c. 235G>A	p. E79K	Heterozygous
M	Esophageal cancer (SCC)	c. 235G>A	p. E79K	Heterozygous
M	Esophageal cancer (SCC)	c. 235G>A	p. E79K	Heterozygous
M	Esophageal cancer (SCC)	c. 239C>A	p. T80K	Heterozygous
F	Esophageal cancer (SCC)	c. 238A>C	p. T80P	Heterozygous
F	Esophageal cancer (SCC)	c. 242G>A	p. G81D	Heterozygous
M	Malignant melanoma	c. 88C>T	p. L30F	Heterozygous
F	Cervical cancer (SCC)	c. 235G>C	p. E79Q	Heterozygous
M	KYSE70: Esophageal cancer (SCC)	c. 72G>T	p. W24C	Homozygous
M	KYSE110: Esophageal cancer (SCC)	c. 246A>T	p. E82D	Heterozygous
M	KYSE180: Esophageal cancer (SCC)	c. 230A>T	p. D77V	Homozygous

Mutant NRF2 Has a Gain-of-Function Activity and Regulates Proliferation and Attachment-Independent Cell Survival in ESC Cells

We compared the transcriptional activities of ESC-associated NRF2 mutants (W24C and D77V) to that of wild NRF2 and determined that mutant NRF2 has a gain-of-function activity, which is partly resistant to KEAP1-mediated inhibition (Figure 2*A*). There was no significant difference in transcriptional activity between homozygous (KYSE30) and heterozygous (KYSE110) mutant cells (Figure W1).

The previously mentioned analysis of clinical samples suggested that *NRF2* mutation plays a role in metastasis and tumor progression of ESC. Exploiting our discovery of ESC cell lines with homozygous *NRF2* mutation, we established KYSE70 cells stably expressing shRNAs against *NRF2* to examine the biologic features solely regulated by mutant NRF2. We tested two different lentiviruses containing NRF2-targeted shRNA (shRNA-1 and -2) along with a control virus. Immunoblot analysis revealed that NRF2–shRNA-2 robustly (11.4% of control) reduced the expression of endogenous mutant NRF2 protein compared with the NRF2–shRNA-1 clone (71.2% of control) (Figure 2*C*). Similarly, NRF2-dependent transcriptional activity markedly decreased (8.9% of control) in shRNA-2 clone (Figure 2*D*).

Table 2. Associations among *NRF2* Mutation Status, Clinicopathologic Factors, and Prognosis.

Clinicopathologic Factor		No. Patients	*NRF2* Mutation, *P*	Overall Survival, *P*	Disease-free Survival, *P*
Sex	Male	69	.914	.119	.656
	Female	13			
NRF2 mutation	+	18	na*	.005	.288
	–	64			
Smoking	+	64	.302	.572	.557
	–	18			
Alcohol intake	+	71	.268	.366	.143
	–	11			
Stage	I-II	25	.709	.895	.038
	III-IV	57			
Invasion depth	>a1	66	.186	.453	.565
	<mp	16			
Lymph node metastasis	+	65	.072	.285	.039
	–	17			
Histologic differentiation	Well	11	.134	.7	.074
	Mod	33			
	Poor	38			
Lymphatic infiltration	+	60	.48	.746	.336
	–	22			
Venous involvement	+	54	.631	.215	.124
	–	28			
Intramucosal metastasis	+	10	.873	.376	.654
	–	72			
Tumor recurrence	+	47	.046	.587	.775
	–	35			

"+" indicates positive; "–," negative; >a1, invade beyond muscularis propria; <mp invade within muscularis propria; well, well differentiated; mod, moderately differentiated; poor, poorly differentiated.
*Not applicable.

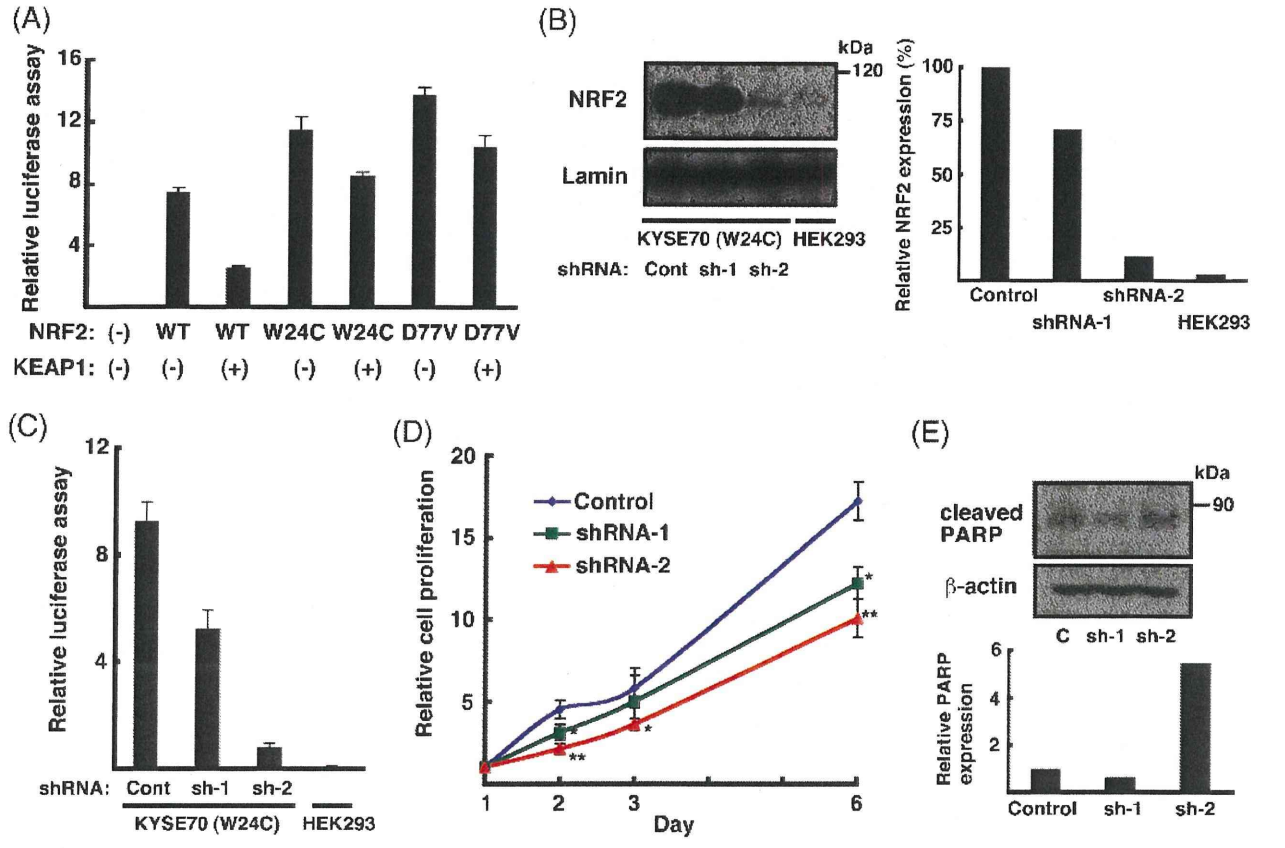

Figure 2. Down-regulation of gain-of-function NRF2 mutant in KYSE70 cells by shRNA. (A) Transcriptional activities of wild-type and ESC-associated mutant NRF2 were measures in the absence or presence of the *Keap1* gene. (B) Down-regulation of NRF2 protein in KYSE70 cells treated with NRF2-targeting shRNAs. Left, Immunoblot analysis of NRF2 protein in the nuclear fraction of KYSE70 cells infected with GFP shRNA (cont) or two different NRF2–shRNAs (sh-1 and sh-2). HEK293 cells lack NRF2 accumulation and were loaded as a negative control. Lamin B1 was used as a loading control. Right, Relative NRF2 expression in each clone was presented. (C) NRF2-dependent transcriptional activities of KYSE clones and HEK293. (D) Cell proliferation plot of KYSE70 clones infected with control or NRF2–shRNAs (shRNA-1 and shRNA-2). Data are mean ± SD of three independent experiments. $*P < .05$, $**P < .01$. (E) KYSE70 clones were cultured on an ultra low-attachment plate for 72 hours, and whole proteins were then extracted. Expression of cleaved PARP was examined by immunoblot analysis. β-Actin was used as a loading control. Relative PARP1 expression compared with the control shRNA was shown below. Molecular marker is indicated on the right (kDa).

Both shRNAs reduced cell proliferation in KYSE70 cells (Figures 2*E* and W2). We then measured attachment-independent cell survival in liquid culture, which mimics the antiapoptotic activity of floating cancer cells in tumor metastasis or recurrence. As shown in Figure 2*C*, only shRNA-2 clones exhibited more apoptosis in culture conditions where adhesion to a substrate was inhibited.

Down-regulation of Mutant NRF2 Increases the Sensitivity of ESC Cells to 5-FU

Previous studies have shown that activation of NRF2 in lung and gallbladder cancers confers resistance to chemotherapeutic drugs [14,15]. To determine whether NRF2 activation has any association with drug resistance in ESC cells, we examined the sensitivity to 5-FU, a commonly used chemotherapeutic reagent for ESC, in ESC cells. We found that NRF2-mutated cells were relatively resistant to 5-FU treatment compared with an NRF2 wild-type cell (Figure W3*A*) and that NRF2–downregulated KYSE70 cells (both shRNA-1 and shRNA-2 clones) showed increased sensitivity to 5-FU (the IC_{50} of each clone was 125.3, 81.3, and 13.1 μM respectively; Figure 3*A*). We also reduced the expression of NRF2 in other *NRF2*-mutated ESC cells using NRF2 siRNA and tested their sensitivity to 5-FU. This yielded results similar to that for KYSE70 cell (Figure 3*B*).

Robust Down-regulation of Mutant NRF2 Is Required for Enhancing Radiation Sensitivity in ESC Cells

Radiation therapy induces oxidative stress by producing reactive oxygen species in cancer cells. Thus, it is very likely that *NRF2* mutation is associated with radiosensitivity. To determine whether mutant NRF2 has a role in acquisition of resistance to irradiation, we exposed control and NRF2 shRNA-infected KYSE70 cells to γ-irradiation (2 Gy) and examined their clonogenic activities (basal colony formation activity of ESC cells is shown in Figure W3*B*), which reflect the degree of irradiation-induced cellular damage. As shown in Figure 3*C*, NRF2-downregulated cells (both shRNA-1 and shRNA-2 clones) were more sensitive to irradiation than control clone. However, when the relative number of colonies was compared among three clones, only the shRNA-2 clone showed a significant reduction ($P = .0002$). This suggests that moderate (~70%) NRF2

down-regulation affected the colony formation activity but that a more complete reduction (~10%) of mutant NRF2 would be required to enhance radiation sensitivity.

It has been reported that the intracellular glutathione level is correlated with sensitivity to radiation [22,23]. To determine whether mutant NRF2 has any role in regulating the level of glutathione in irradiated ESC cells, we measured the expression of major enzymes (glutamate-cysteine ligase, catalytic subunit [GCLC] and glutathione reductase [GSR]), which regulate glutathione synthesis and modification and are direct targets of NRF2 [21,24], in NRF2-downregulated KYSE70 cells exposed to various doses of irradiation. Quantitative RT-PCR analysis revealed that down-regulation of mutant NRF2 (shRNA-2 clone) was significantly reduced not only for the inducible expressions of GCLC and GSR but also for their basal level (Figure 3*D*). Interestingly, this reduction was not obvious in the shRNA-1 clone, which is consistent with the radiation sensitivity experiment previously mentioned and suggests that robust NRF2 down-regulation would be required for decreasing glutathione-regulatory enzymes (Figure 3*D*). Consistently, the basal level and radiation-induced increase of reduced glutathione were diminished only in the shRNA-2 clone (Figure W4).

Molecular Signatures Associated with NRF2 *Mutation Are Prognostic Factors for ESC and Predictive of Response to CRT*

These *in vitro* data strongly suggested that NRF2 activation by genetic alteration could be associated with the clinical response to CRT. However, the previously mentioned ESC cohort, whose *NRF2* mutation status was determined, contained only eight cases that had received postoperative CRT. Despite the difficulty in obtaining molecular data from minute biopsy samples of tumors before treatment, we

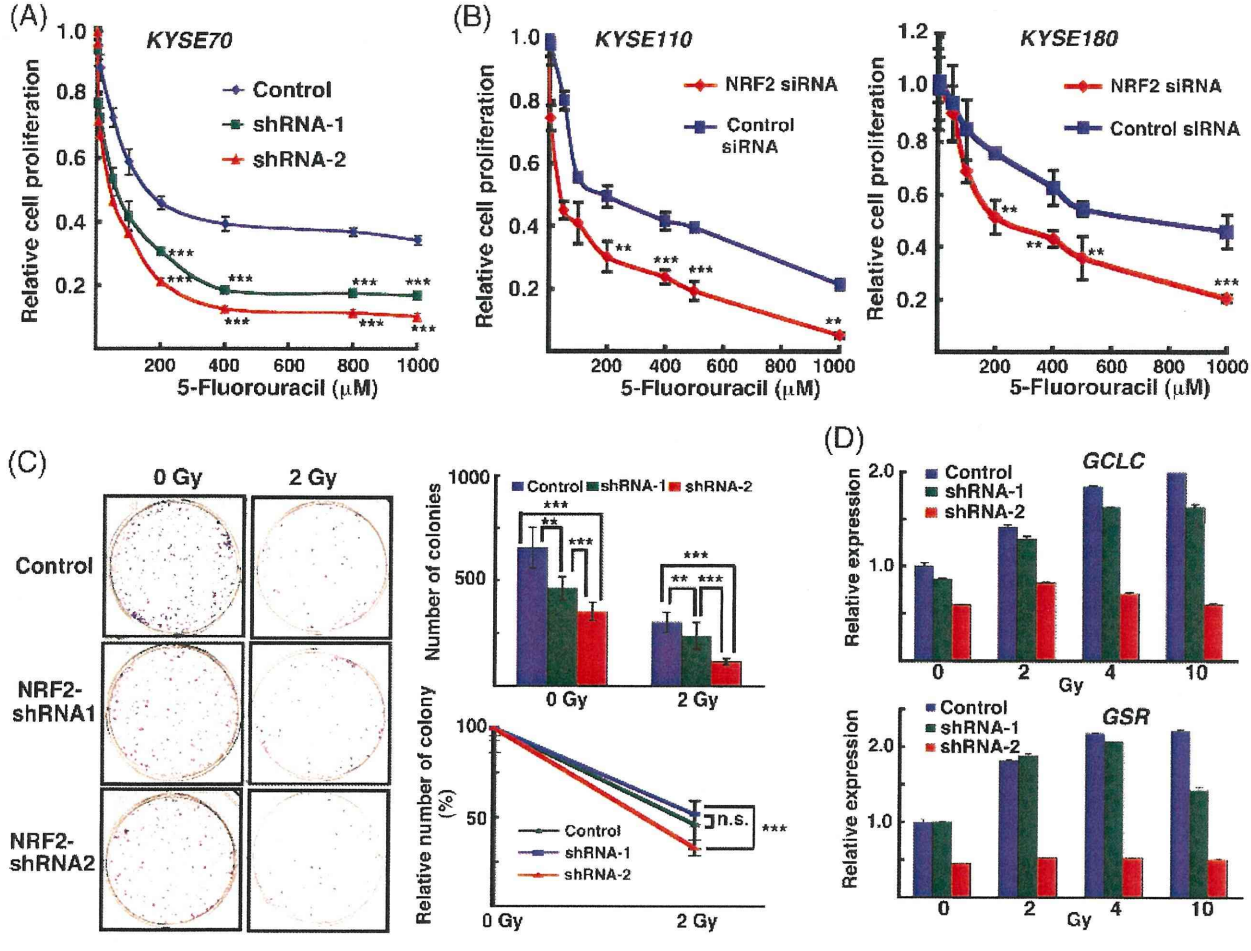

Figure 3. Mutant NRF2 confers resistance to chemotherapeutic reagent and radiation. (A) KYSE70 clones infected with control shRNA or NRF2–shRNAs were treated with various concentrations of 5-FU. (B) KYSE180 and KYSE110 cells were treated with control or NRF2 siRNA and various concentrations of 5-FU, as in A. Data represent cell viability after 48 hours relative to vehicle (DMSO)-treated control. Data are mean ± SD of three independent experiments; statistical difference to control siRNA or shRNA, $^{**}P < .01$, $^{***}P < .001$. (C) Left, A representative plate showing colony formation by each clone with control (0 Gy) and 2-Gy irradiation. Top right, Number of KYSE70 clones infected with control shRNA and NRF2–shRNAs that formed colonies after control (0 Gy) and 2-Gy irradiation. Data are mean ± SD of eight independent plates. Bottom right, The relative number of colonies after 2-Gy irradiation compared with the control (0 Gy). Note that the difference between control shRNA and shRNA-1 clones was not significant (n.s.). (D) KYSE70 clones were irradiated with different doses, and the expression of GCLC and GSR mRNAs was then examined. Data are mean ± SD of three independent experiments, $^{**}P < .01$. $^{***}P < .001$.

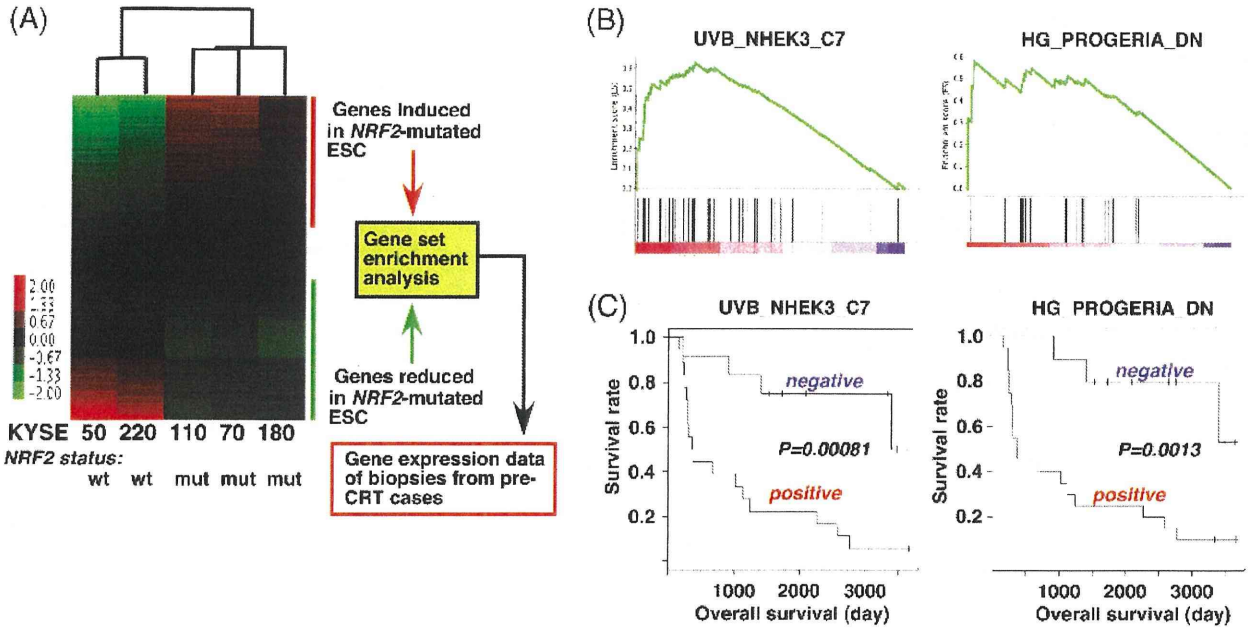

Figure 4. Pathway signatures of mutant NRF2 are associated with ESC patients' survival after CRT. (A) Two-dimensional hierarchal clustering of KYSE cells by genome-wide gene expression. NRF2 mutation status is shown at the bottom. GSEA extracted characteristic gene sets enriched in NRF2-mutated or wild-type ESC cells, and their prognostic significance was evaluated based on gene expression data for biopsies from pre-CRT cases. (B) Representative panels showing results of GSEA of genes enriched in NRF2-mutated ESC cell lines. (C) Kaplan-Meier plot showing overall survival of ESC patients after CRT segregated according to the NRF2 mutant signature.

previously collected the gene expression profiles of 33 pre-CRT samples of ESC for which the same therapeutic protocol had been used and for which the therapeutic response had been clinically evaluated [25]. Therefore, using this data set, we attempted to analyze whether the gene expression signatures associated with *NRF2* mutation could be predictive markers of response to CRT in ESC.

For this purpose, we first obtained the genome-wide gene expression data for five ESC cell lines and extracted the *NRF2*-mutated ESC signature based on the *NRF2* mutation status (Figure 4*A*). Using GSEA, we obtained a panel of molecular pathway signatures that were significantly associated with *NRF2* mutation status (representative pathways are shown in Figure 4*B*). The expressions of 703 gene sets were increased, and those of 14 gene sets were decreased in *NRF2*-mutated ESC cell lines (a complete list is shown in Table W3). We then tested whether changes in the expression of any of these signatures were associated with the clinical response to CRT and overall survival after treatment. We found that the increased expression of 15 gene sets was significantly ($P < .05$) associated with both poor response to CRT and a poor patient outcome after CRT (Table 3; representative Kaplan-Meier plots are shown in Figure 4*C*). All of the potentially predictive molecular signatures were increased in *NRF2*-mutated ESC cell lines and included pathways related to the oxidative stress response ($n = 4$), immune/cytokine response ($n = 4$), and hematopoietic disorder ($n = 3$) (Table 3). We further elucidated that direct NRF2 target genes confirmed by a combination of ChIP-seq and microarray analysis [21] were significantly

Table 3. Mutant NRF2 Signatures Associated with CRT Response.

Molecular Pathways	Prognosis, *P*	Clinical Response, *P*	NRF2 Target Enrichment, *P*	No. NRF2 Target Genes	Functional Annotation
ET743PT650_COLONCA_DN	.000103	.00404	.000917	7	Anticancer drug
GLYCOSPHINGOLIPID_METABOLISM	.000744	.00519	.585	1	Glycolipid metabolism
UVB_NHEK3_C7	.000813	.0235	.00279	7	Oxidative stress response
HG_PROGERIA_DN	.00132	.0109	.6	1	Aging
TAKEDA_NUP8_HOXA9_16D_UP	.00306	.0186	.318	8	Hematopoietic disorder
CARIES_PULP_HIGH_UP	.00466	.0186	.865	2	Immune/cytokine response
ABRAHAM_AL_VS_MM_UP	.0083	.00688	.254	2	Hematopoietic disorder
ABRAHAM_MM_VS_AL_DN	.0083	.00688	.24	2	Hematopoietic disorder
IFN_GAMMA_UP	.00847	.045	.165	3	Immune/cytokine response
AS3_FIBRO_C4	.00865	.0235	1	0	Oxidative stress response
TSADAC_RKOSILENT_UP	.0115	.045	.52	1	Methylated in colon cancer
BRCA1KO_MEF_DN	.0144	.0174	.0267	7	Oxidative stress response
UVB_SCC_DN	.016	.0235	.899	2	Oxidative stress response
CMV_HCMV_TIMECOURSE_24HRS_DN	.0196	.045	.0169	5	Immune/cytokine response
SANA_TNFA_ENDOTHELIAL_UP	.0286	.00669	.587	3	Immune/cytokine response

Table 4. NRF2 Target Genes Enriched in the CRT-predictive Pathways.

Pathway	Gene Symbol	Gene Name
ET743PT650_COLONCA_DN	*MGMT*	O^6-methylguanine-DNA methyltransferase
	LRBA	LPS-responsive vesicle trafficking, beach, and anchor containing
	KIFAP3	Kinesin-associated protein 3
	IRS1	Insulin receptor substrate 1
	GBE1	Glucan (1,4-alpha-), branching enzyme 1 (glycogen branching enzyme, Andersen disease, glycogen storage disease type IV)
	ADK	Adenosine kinase
	BRE	Brain and reproductive organ-expressed (TNFRSF1A modulator)
UVB_NHEK3_C7	*PGD*	Phosphogluconate dehydrogenase
	ESD	Esterase D/formylglutathione hydrolase
	ADK	Adenosine kinase
	PAM	Peptidylglycine alpha-amidating monooxygenase
	AKR1A1	Aldo-keto reductase family 1, member A1 (aldehyde reductase)
	CDKN3	Cyclin-dependent kinase inhibitor 3 (CDK2-associated dual-specificity phosphatase)
	PLA2G4A	Phospholipase A2, group IVA (cytosolic, calcium-dependent)
BRCA1KO_MEF_DN	*PDIA4*	Protein disulfide isomerase family A, member 4
	GPT2	Glutamic pyruvate transaminase (alanine aminotransferase) 2
	MAN1A1	Mannosidase, alpha, class 1A, member 1
	LAMC1	Laminin, gamma 1 (formerly LAMB2)
	ADD3	Adducin 3 (gamma)
	CDC2L6	Cell division cycle 2-like 6 (CDK8-like)
	KLF9	Kruppel-like factor 9
CMV_HCMV_TIMECOURSE_24HRS_DN	*WNT5A*	Wingless-type MMTV integration site family, member 5A
	SERPINE1	Serpin peptidase inhibitor, clade E (nexin, plasminogen activator inhibitor type 1), member 1
	ANXA1	Annexin A1
	VEGFC	Vascular endothelial growth factor C
	ADD3	Adducin 3 (gamma)

enriched in part of these pathways (Table 2; enriched genes are listed in Table 4).

Discussion

NRF2 *Mutation in ESC*

In the present study, we conducted mutation screening of the *Nrf2* gene in a wide range of tumor types including sarcoma and found that *NRF2* mutation is specifically frequent in EC and rarely occurs in cervical cancer and melanoma. These ESC-associated mutations harbor gain-of-function activity. Because *Keap1* recognizes two distinct regions of NRF2, single amino acid change may not completely inhibit *Keap1*-mediated degradation or sequestration [19]. Recently, Kim et al. [26] performed a mutation screening of hot spots in the *Nrf2* gene in more than 1000 tumors and reported that *NRF2* mutation is recurrent in tumors of the lung, skin, esophagus, and larynx, which is concordant with our previous and current observations. We previously reported that *NRF2* mutation was more common in smoking-associated lung cancer [19]; however, we failed to demonstrate any significant association between the presence of *NRF2* mutation and smoking history ($P = .302$) in ESC, probably because most of the affected patients in our cohort (64/82, 78%) were smokers. Also, *NRF2* mutation status was not associated with the habitual alcohol intake ($P = .268$). Previous genetic analyses have shown that polymorphisms of the *GSTP1* and *NQO1* genes, both of which are known direct targets of NRF2, are associated with susceptibility to ESC in Asian and white populations [27–29]. It would be interesting to examine the frequency of *NRF2* mutation in other ESC cohorts with different genetic, epidemiological, or ethnic backgrounds.

Because *Keap1*-deleted mice show hyperkeratosis in the forestomach [30], which is analogous to the esophagus, NRF2 activation could affect differentiation process of esophageal epithelium, which might be associated with malignant features of ESC. Our analysis of a cohort of ESC cases has further revealed the clinical significance of *NRF2* mutation. Our mutation analysis revealed that *NRF2* mutation was only detected in the late stage ESC. The presence of *NRF2* mutation was associated with tumor recurrence and was shown to be a significant prognostic factor. A recent study aimed at identifying NRF2 target genes by ChIP-seq has revealed that NRF2 directly regulates the expression of gene groups that are related to cell proliferation and survival, in addition to the detoxification response [21]. Using ESC cell lines containing *NRF2* mutation, we found that mutant NRF2 promotes ESC cell proliferation. We further revealed that mutant NRF2 confers attachment-independent cell survival, which is intimately associated with lymph node metastasis and tumor progression. Collectively, our results demonstrate that aberrant NRF2 activation resulting from its genetic alteration occurs at a relatively advanced stage of ESC and that it induces cell proliferation and survival signals, resulting in acquisition of malignant features and poor prognosis.

Molecular Signature of NRF2 *Mutation and Chemoradiation Therapy in ESC*

In addition to these malignant characters of cancer cells, resistance to current therapies would also be associated with a poorer survival rate. Previous studies have shown that NRF2 activation by loss-of-function mutations or down-regulation of the *Keap1* gene confers resistance to chemotherapeutic drugs and radiation [14,15,18,31]. As has been reported in lung cancer [19], down-regulation of mutant NRF2 enhanced the sensitivity of ESC cells to a chemotherapeutic agent. Furthermore, mutant NRF2 regulates resistance to irradiation partly through induction of enzymes related to glutathione synthesis. Consequently, effective inhibition of aberrant NRF2 signaling could offer a novel therapeutic approach for ESC in combination with CRT. Interestingly, robust reduction of mutant NRF2 was required to inhibit